AD636680

MECHANISMS OF LASER-SURFACE INTERACTIONS

By

J. F. Ready

E. Bernal G.

L. P. Levine

FINAL REPORT

To

Ballistic Research Laboratories

Contract No. DA-11-022-AMC-1749(A) Mod. No. 2

May 1966

D D C

AUG 1 5 1966

C

HONEYWELL
/ Corporate Research Center

MECHANISMS OF LASER-SURFACE INTERACTIONS

By

J. F. Ready

E. Be. nal G.

L. P. Levine

FINAL REPORT

To

Ballistic Research Laboratories

Contract No. DA-11-022-AMC-1749(A) Mod. No. 2

May 1966

Presented by

Honeywell Inc.
CORPORATE RESEARCH CENTER
Hopkins, Minnesota

TABLE OF CONTENTS

LIST OF ILLUSTRATIONS

INTRODUCTION

This report describes investigations of the interaction of high power laser radiation with surfaces using a time-of-flight mass spectrometer and a quadrupole mass spectrometer. The work described in this report builds on and extends results already reported in the semi annual report[1] on this same project. Since some phases of the investigations are already completely reported there, we will not duplicate that material. For background, however, some of the earlier developments upon which this report depends are summarized below.

Earlier work involved measurements of the ions emitted from tungsten targets and was carried out with a time-of-flight mass spectrometer. The species emitted at a laser power per unit area of the order of 50 megawatts/cm^2 included sodium, potassium, and tungsten. The ions were found to possess energies up to 200 ev per ion.

Neutral gas desorption was observed earlier using a quadrupole mass spectrometer. The dominant species found were adsorbed gases such as CO and CO_2, in quantities of the order of 10^{12} molecules per pulse. This amount, and also the manner in which the number of desorbed molecules varies with laser power, agrees well with a thermal interpretation of this phenomenon in which the heating of the surface by the laser beam drives off adsorbed gases. Theoretical work on possible heating of the blow-off material, because of absorption of laser light in inverse Bremsstrahlung processes in the field of the ionized atoms, indicated heating is probable at high particle densities, but it does not occur at particle densities representative of our experimental conditions.

In this report we describe continued work on the two spectrometers. We have employ d targets of different materials, and obtained results generally similar to those found with tungsten targets. The two largest topics in this report involve measurements on high energy neutral particles in the quadrupole spectrometer, and analysis of the pulse shapes of the ions emitted in the time-of-flight spectrometer, in order to infer the velocity distribution of the original material. These two topics have occupied much of the present report period and, correspondingly, fill much of this report.

Section I discusses the high speed neutral particle emission. These pulses appear rapid compared to the longer and slower pulses from the gas desorption work. We shall consider the various experiments designed to establish the nature of this emission. We show that the surface interaction produces ultraviolet radiation at wavelengths down to 1100A° , and high speed neutral atoms or molecules with energies of the order of 100ev. Definite identifications of the atomic or molecular species have not yet been attained.

In Section II we describe the experiments done on the time-of-flight spectrometer. The main items here are investigations on platinum targets, and an experiment in which time of flight of the ions was measured as a function of accelerating voltage as an additional check on the validity of the theory of operation of the spectrometer.

In Section III we analyze tne pulse shapes obtained with the time-of-flight spectrometer, and obtain distributions that indicate a directed component of the ion energy, plus a smaller random component superposed on the directed component.

Typical results indicate that the energies are of the same order of magnitude, but not equal, for ions of different species emitted from a given target. The shapes of the velocity distributions indicate departures from a Maxwellian distribution. The computational procedure used here rests on an analysis developed by Frank J. Allen of Ballistic Research Laboratories which we have programmed for a computer and used to obtain velocity distributions from the ion pulse. We include Allen's results as appendix I in order to make this report self-contained. Much of the discussion in Section III depends on Allen's report which is not generally available. In the appendix we have condensed Allen's original document, retaining only those portions which have the most relevance for this report.

Finally, as Appendix II we include a copy of a paper based on work performed under this contract and presented at the Fourth International Quantum Electronics Conference in Phoenix, Arizona, April 12-15, 1966. It draws mainly on results presented previously in the semi-annual report[1]. We include it here because it forms a concise and unified statement of work that has been performed under this contract.

I. WORK ON QUADRUPOLE MASS SPECTROMETER

This section discusses work done on the quadrupole mass spectrometer during the report period.

The main work on this instrument involved the study of high energy molecules emitted from metallic targets upon illumination by the laser.

A. OBSERVATION OF THE HIGH SPEED NEUTRAL MOLECULES

During our study of the gas desorption reported earlier, a pulse was noted occurring simultaneously with the laser event. Since these data were taken with a very slow time sweep, it was not possible to determine if the pulses were as long as several tens of milliseconds or shorter. Since UV light and high speed ions had already been observed in the time-of-flight spectrometer, it seemed reasonable that the pu's observed was due to either of those effects. A study was made to determine which it was. When the pulse was observed in higher time detail, it had an appearance typified by the data shown in figure I-1. (In this figure, time progresses to the right at 10 microseconds per centimeter, and the negative going signals extend upwards with a sensitivity of 10^{-5} amps per cm.) The sweep is triggered by the laser event; not by the first pulse of the train. The first pulse is quite high and short, beginning with the laser event, and has a width consistent with the time constant of the detection system (R = 200 ohms and C = 50 pf). The second pulse begins to rise 5 μsec after the laser event and has a width of about 7 μsec. Later and wider pulses also appear. When these data were observed, several experiments were performed to determine if the pulses resulted from ultraviolet light, high speed ions, or high speed atoms.
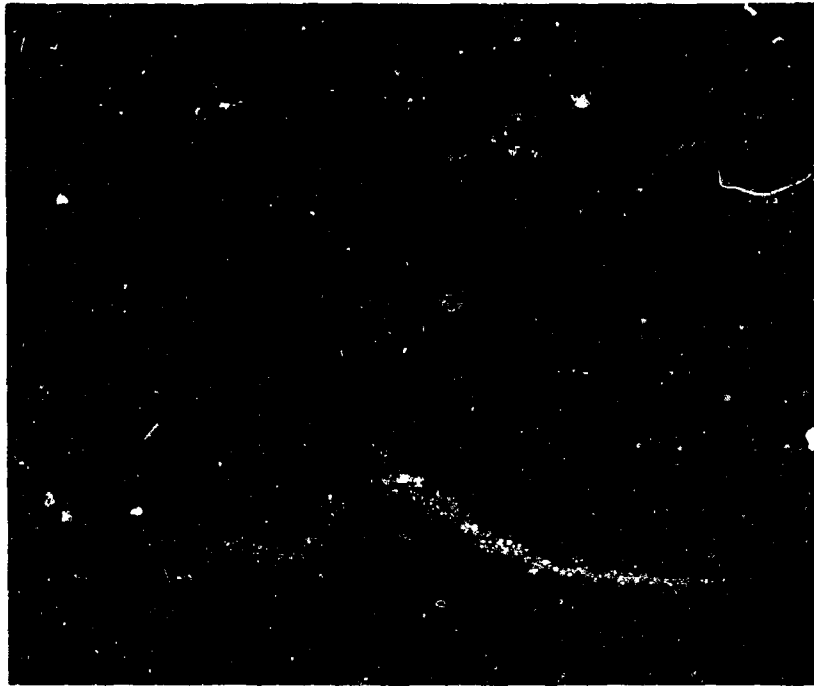
Figure I-1 - Photon Pulse and High Speed Molecule Pulse from a Tungsten
Target. Time progresses to the right at 10 microseconds/cm.

B. DETECTION MECHANISM FOR HIGH SPEED MOLECULES

Photons, high speed atoms, and high speed ions all arrive at the detector much sooner than do ions resulting from room temperature gases generated by the laser beam. Photons, if they have a high enough energy, and ions of nearly any velocity can be detected directly at the multiplier. High speed neutrals, on the other hand, pose a special problem.

When one is working with gas phase neutral molecules moving with speeds corresponding to thermal motion at room temperature, the detection mechanism usually involves the ionization of the atom or molecule followed by the sub-sequent mass analysis and detection of the ion. Under these conditions the density of the atoms in the gas phase can be inferred from the known ionization probability by electron impact and the electron beam current. About 1 atom in 10^8 generated is usually detected.

When high speed atoms or molecules are encountered, the same techniques should work in principle. However, the speed of the atoms, and the fact that they reside in the ionizing region a very short time, make the number of ions formed by electron impact very small compared even to that for room temperature conditions. Because of the enormous kinetic energy of the high speed atoms, the time spent in the ionization region is very small (inversely proportional to velocity). Furthermore, the kinetic energy is dissipated on the very first collison with a wall. Thus the probability of detecting a high speed atom or molecule by this technique is many orders of magnitude lower than that of detecting thermal atoms and molecules.

For atoms of high energy, however, there is at least one detection mechanism which depends in no way on ionization by an electron beam. In this scheme the atoms are allowed to strike a surface and produce secondary electrons. The secondaries are then detected by conventional means. In our system the atoms are allowed to strike the first dynode of the electron multiplier detector, and the resulting secondary electrons traverse the multiplier, building up into an easily detectable signal.

The number of atoms in the initial beam can be computed if one knows the gain of the electron multiplier and the value of Y, the coefficient for secondary electron production by the neutral atoms at the target surface. There are very few estimates of Y in the literature. One by Rostagni[2] is reproduced in table I-1. In it he shows a secondary electron coefficient of 0.07 for argon atoms of 200 ev energy. For neon and helium he estimates 0.04 and 0.39 respectively. Estimates or calculations for other gases or for specific surfaces are not available. Also reproduced as part of table I-1 are data from the same source on Y for ion impact. Note how the values of Y are essentially identical for values of kinetic energy greater than 200 ev. Thus, for energies greater than 200 ev, it should be possible to infer the atomic secondary effects from the value of y for ions on surfaces (At high kinetic energies the charge of the particle should be of small importance when collision parameters are involved). Brown[3] gives a good summary of values of Y in the literature for ions on various surfaces. He indicates that values of Y of the order of 0.02 through 0.2 for energies greater than 200 ev are the rule.

Since we will be discussing the interaction of hydrogen atoms or molecules with beryllium-copper dynodes, it will be necessary to estimate the variation of Y with atomic or molecular kinetic energy. Some sort of picture such as the following may be suggested: The value of Y for energy less than some value (perhaps 200 ev) is linear with energy. Above that energy Y is constant.

TABLE I-1

VALUES OF THE SECONDARY ELECTRON COEFFICIENT γ

E (ev)

	600	400	200	100	50	30	25	20
Ar	23.2	17.0	7.0	1.3	0.4	0.02	0.008	
Ne		7.3	3.6	1.0	0.3	0.02		
He		43.5	39.3	8.1	0.8	0.06		0.008

E (ev)

	600	500	400	300	200	100	50	30	25	20	16	11	6
H_2^+		55	51	36	19	8.5	3.3						
Ar^+	31		20		8	3.3	2.5	2.9	2				
Ne^+			25		17	13.0	9.0	8.0		6.0	5.2	5.1	
He^+			57		38	26.0	20.0	18.0		16.3	17.2		16.6

This picture is consistent with the assertion that the kinetic energy of the atom or ion is the major fraction of the excitation if it is large compared to the work function of the surface, and that the excitation by an uncharged particle is zero at zero kinetic energy. When we wish to interpret the pulses of high speed atoms in relative numbers, we shall have to use such a picture; however, for this report we shall state only that this problem of the variation of Y with atomic kinetic energy is a serious one.

C. USE OF THE QUADRUPOLE MASS ANALYZER TO DETERMINE THE NATURE OF THE HIGH SPEED PULSE TRAIN

The quadrupole mass spectrometer is ideally suited to determine the nature of the train of pulses observed in this experiment. It has been described in a previous report[4]. Since it is a spectrometer with a line-of-sight path between the ion source and the detector, and since the detector is an electron multiplier capable of detecting any particle creating secondary electrons, it will allow high speed ions, excited or high speed atoms, and photons to travel from the target to the detector and be observed. In order to separate the different possible effects, subsidiary experiments must be performed. These experiments depend on the forces which can be applied to different kinds of particles.

1. Charged Particles

The mass spectrometer should remove from the beam any charged particle of a charge-to-mass ratio other than that for which it is in resonance. However, for high energy ions or electrons, the transit time may be smaller than that required for the mass filter to act. For ions, this energy is greater than 200 ev. (Mass spectra have been taken with ion energies of up to 400 ev and the filter is effective at this energy). Thus, for ions up to 200 ev initial energy, the mass spectrometer set to be electronically opaque

should stop all ions. Electrons of relatively low energy will have sufficient velocity to traverse the spectrometer without being filtered. These electrons would, however, not be able to strike the first dynode of the multiplier unless they had at least 3000 ev of energy. Thus, setting the spectrometer to be electronically opaque should stop all charged particles of less than 200 ev. In addition, a magnetic field of approximately 500 gauss can be applied externally to the spectrometer housing crosswise to the path of the particles. Such a magnetic field will give even high energy ions curvature of path following the equation:

$$R = \left[\frac{144 \ mE}{eB^2} \right]^{1/2}$$

where R is the radius of curvature of the trajectory in cm, E is the particle energy in ev, B is the field in gauss and e/m is the charge to mass ratio in electronic charge/atomic mass units. For B = 500 gauss, E = 200 ev and e/m = 1/50 e/amu, R is about 2 cm. Since this 500 gauss field could be applied over an area encompassing at least 5 cm of particle path length, it should be possible to stop relatively fast ions with it as well as with the mass filter. In the experiments to be described below both methods are used.

2. Photons

If photons are emitted from the point of impact of the laser light, some of them will strike the first dynode of the electron multiplier and will be detected via secondary electron effects. The photons will require an energy greater than the work function of the beryllium-copper dynode. This energy is not well known but should be equivalent to ultraviolet radiation, as the multiplier is known to be insensitive to the white hot filament in the ion source of the mass spectrometer. Energy analysis of the photons may be accomplished

by passing them through a filter. For crude analysis, rather simple filters may be used such as quartz (passes wave-lengths longer than 2000Å),lithium fluoride (cutoff at 1100Å), barium fluoride (cutoff at 1350Å), and pyrex (cutoff at 2800Å). Experiments are discussed below using these filters to give the approximate spectrum of the ultraviolet radiation emitted. The spectrum must be corrected for the wavelength dependence of the photoelectric yield of the first dynode of the detector.

3. Uncharged Particles

3.   Uncharged Particles

Uncharged particles of atomic dimensions can be stopped only by interposition of a physical barrier. Materials such as quartz may be used which will pass ultraviolet radiation but stop uncharged (as well as charged) species. Since no moderate fields will deflect uncharged particles, they will pass through the spectrometer undeflected and will be detected by the electron multiplier if the kinetic energy is sufficient to cause secondary emission from the surface of the first dynode of the multiplier. We will assume that this will be true for atoms of energy greater than approximately 50 ev. In the event that the atoms are excited, however, the energy of excitation will be available for secondary electron ejection, causing detection at even lower kinetic energies. Since these atoms will be moving at considerably slower speed, they will arrive quite late after the photon pulse. The kinetic energy (not including energy of excitation) of high-speed atoms can be inferred, if one knows the mass of the atom, from the time of flight of the atom from its source to the detector. For a mass of m amu and for a kinetic energy of E electron volts, the time in seconds for a flight of d cm is:

$$t = 10^{-6} d \ [m/2E]^{1/2}$$

which, for m = 1 amu, d = 60 cm and E = 200 ev, results in t = 3 μsec. For m = 1 amu, d = 60 cm and E = 50 ev, t = 6 μsec. Thus, the results of having a spread of ion energies from 0 to 200 ev will result in a peak from 3 to 6 μ seconds after the initiation of the pulse of high speed atoms. (No consideration of atoms slower than 50 ev is taken because the secondary electron emission is very small for energy less than 50 ev.) It is, of course, impossible to accelerate or decelerate the atoms so they cannot be separated by electric fields as are the ions in the time-of-flight spectrometer.

D. STUDY OF THE HIGH SPEED NEUTRAL MOLECULES

In our December 13th progress report we discussed the first observation of what were possibly high-speed neutral molecules emitted from the laser target. At that time it was clear that there was some sort of signal which was occurring very shortly after the laser burst, and which was apparently unaffected by any applied fields.

Since that time considerable work was done to determine just what these pulses were. Our conclusion is the following: When a Q-switched laser beam strikes a target surface, there is an immediate burst of ultraviolet light extending down to wavelengths of the order of 1100Å accompanied by an emission of neutral molecules of atomic weight of 1 or 2 amu and up. These neutral molecules have energies of the order of 100 ev.

A typical trace taken from the data is shown as figure I-1. None of the pulses shown disappear when the spectrometer is set to be electronically opaque or when a crossed magnetic field of 500 gauss is applied; therefore, one may conclude that they are not caused by charged particles of either sign. These peaks are, therefore, due to high speed atoms, excited atoms, or photons.

1. The Photon Pulse

We have shown that the first peak in this picture is a photon pulse. The experiment used to show this involves the use of filters of LiF, BaF_2, quartz, and pyrex. Table I-2 shows the height of this peak when filters of these materials are interposed between the target and the electron multiplier detector. Note that this is not meant to be the UV emission vs wavelength but the product of the UV emission times the quantum efficiency of the first dynode vs wavelength. It should be noted that the height of this peak decreases as the cutoff wavelength of the filter is made longer. The fact that there is some amplitude of this pulse when pyrex glass is used as a filter should not be used to infer that there is radiation of wavelength longer than $2800 \overset{o}{A}$. The filter does not block all paths from the target to the detector, only direct ones; so there may well be some reflected UV passing around the filter. The data show that the height of the first pulse varies monotonically with the power density of the laser illumination of the target. The fact that the first pulse of the train (1) has a height which varies monotonically with the illumination density, (2) is not changed by interposing electric or magnetic fields between the target and the detector, (3) is decreased in intensity in agreement with the characteristics of known UV filters, and (4) occurs coincidentally with the laser burst, establishes without doubt that it is due to ultraviolet light emitted by the target upon irradiation by the Q-switched laser beam.

2. The High Energy Neutral Molecule Pulses

Following the pulse of photons in figure I-1, are three other pulses. We have shown that none of these pulses is affected by (1) making the spectrometer electrically opaque, (2) applying a crossed magnetic field, or (3) applying positive or negative potentials to the target. They can be made to dissappear,

TABLE I-2

TRANSMISSION OF THE FIRST PULSE (PHOTON PULSE)
FOR VARIOUS FILTERS

FILTER MATERIAL	APPROXIMATE UV CUTOFF (Å)	AMPLITUDE OF FIRST PULSE AS FRACTION OF AMPLITUDE WITH NO FILTER
LiF	1100	0.7
BaF$_2$	1350	0.5
QUARTZ	2000	0.3
PYREX	2800	.01-.02

however, by interposing any of the UV filters described above between the target and the detector. Furthermore, they are delayed in time from the laser burst by times in excess of 2 μsec. This set of conditions makes it certain that these pulses are due to high energy neutral particles.

The first of these pulses can be shown to be either due to neutral hydrogen atoms with kinetic energies of the order of 100 ev, or some other neutral particle with even higher energy. As we have shown in Section I-C-3 the time of flight of a neutral particle of mass m amu and with energy E ev over a distance d cm is, in seconds:

$$t = 10^{-6} d [m/2E]^{1/2}$$

Thus, for a given time of flight, an increase in m must be accompanied by a proportional increase in E. Since the first of the pulses we have called the neutral particle pulses begins to arrive at the detector only 5 μsec after the laser burst, and since the detector is 60 cm from the target, the particle must have either a mass of 1 amu (the smallest mass possible for a neutral particle) and a kinetic energy of 70 ev, or a mass greater than 1 and even larger energy. The data reported does not permit any other possibilities.

3.   Mass Discrimination Efforts in the High Speed Neutral Molecule Pulses

It is not possible to accelerate atoms by fields. As a result, it is not possible to determine separately the energy and mass of the high speed atoms as can be done with the high speed ions. It is possible, however, to determine a minimum mass-maximum energy crossover for a given peak and to match peaks from a given laser burst for energy and mass possibilities.

This sort of analysis is carried out in Section II using typical data taken with this apparatus.

E. STUDIES ON HIGH ENERGY MOLECULES

High energy molecules have been observed, thus far, emanating from tungsten, single crystal nickel, and titanium. Tungsten was studied because it was the metal on which the bulk of our work was performed. When the high energy atoms were detected emanating from tungsten, it became clear that some other metal would have to be used to determine the species since it is well known that all kinds of gas can reside on a surface of polycrystalline tungsten. It was decided to use as our target two kinds of surfaces - single crystal (100) nickel and polycrystalline titanium.

Work by D. Lichtman in our laboratory has shown that single crystal (100) nickel seems to have hydrogen as its only gas coverage. When different gases are admitted into his vacuum system and electron induced ion desorption is attempted, only ions resulting from hydrogen desorption have ever been observed. Thus, it was hoped, only one species of high speed atom or molecule would be detected in the laser induced desorption experiment with (100) nickel, and that species would be of mass 1 or 2 amu. With only one species of desorption, the analysis of the energy of the atom or molecule would be quite simple. Titanium, on the other hand, can be covered by a wide range of gases. In fact, the surface is so active chemically that all but the rare gases are chemically bonded to the surface. Of these gases, only hydrogen is bonded reversibly. It was felt that with titanium as a target, the usual array of high speed atom pulses would be observed, but that only one of them - the first in time - could be made to vanish as the target was heated to a temperature in excess of 300° C.

The studies on the nickel target were inconclusive. When the laser beam was allowed to strike the target, peaks were observed which could not be interpreted in terms of only one species of gas on the target. When gas desorption data were taken, it was found that both hydrogen gas and carbon monoxide gas were desorbed. When the surface was heated to as high as 700° C (a temperature above that at which hydrogen was found by Lichtman to desorb from the surface), the first peak of the high-speed atom group vanished at times and remained at others. The crystal was removed from the vacuum system and subjected to X-ray diffraction analysis. It was found that the region struck by the laser had been melted and refrozen in a polycrystalline form. The data were therefore totally in agreement with what could have been the case for polycrystalline material.

When titanium was used as a target, the results were somewhat more conclusive. The data had generally the appearance of 3 or 4 peaks. The first peak did in fact come and go as a function of the temperature of the target, and the other peaks did not. Figure I-2 shows typical data for a titanium target. In both I-2a and I-2b, time goes to the right. In each case the top trace (signal extending downward) has a speed of 2 μsec/cm and a sensitivity of 10^{-3} amps/cm. The lower trace (signal extending upward) has a speed of 5 μsec/cm and a sensitivity of 4×10^{-3} amps/cm. Figure I-2a is for a cold titanium target. Figure I-2b is for a hot titanium target. The only important difference between them is a disappearance of the second peak from the left in figure I-2b.

It was not possible, however, to establish the presence or absence of gaseous hydrogen desorption as a function of target temperature which correlated with the high speed atom data. (The reflected laser energy for these runs was inadvertently allowed to strike an interior metal surface instead of the exit window as had been designed. Gas from the surface struck by this unfocused but still intense beam could easily have confused the data. Work is now underway to correct this.) With the

(a) Cold Target
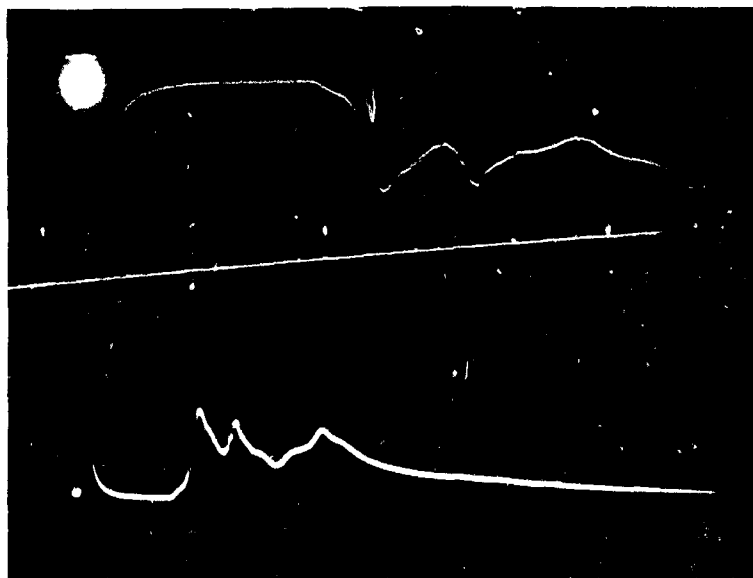
(b) Hot Target

Figure I-2 -   Photon Pulse and High Speed Molecule Pulse from a Titanium
Target. In each photograph top trace, negative signal downward; bottom
trace, negative signal upward. Time progresses to the right. Upper trace:
2 microseconds/cm. Lower trace: 5 microseconds/cm. (a) Cold Target
(b) Hot Target.

titanium data it is now clear that the presence and absence of the first peak of the high-speed atom group can be correlated with the temperature of the titanium target. Although the actual temperature at which this peak disappears is not yet known, it is in a range which correlates with the degassing of the titanium hydride. The other peaks remain unaffected by the thermal treatment of the target. This is in agreement with the interpretation of these peaks as due to other nondesorbing gases, and even to the base material itself.

F. THE TOTAL NUMBER OF MOLECULES EMITTED FROM THE TARGET

An estimate may be made of the total number of atoms of a particular species emitted from the target during a laser burst if one knows the value of γ for the species on beryllium-copper and the spatial distribution of the high speed atoms. In our case neither of these is known with even crude precision. However, we can say that for the energy range of interest, γ is in excess of 0.01 and that the spatial distribution is approximately isotropic. Using these two factors, and the height and time duration of the pulse coupled with the gain of the multiplier (of the order of 10^4), we can arrive at the total number of atoms emitted. A typical pulse, pulse 1 of figure I-1, is of the order of 0.01 volt high with an input resistor of 500 ohms. Simple calculation shows that this signal is equivalent to 10^6 electrons emitted from the first dynode of the electron multiplier. With a value of γ equal to 0.01, this implies that 10^8 high speed atoms arrived at the detector. The detector has an active area of less than 1 cm^2 and is 60 cm from the target. If one assumes that the emission of high speed neutrals is isotropic over a hemisphere, the total number of high speed atoms emitted is 3.6×10^{11}. This number is quite high when compared with the number of high speed ions observed. It can be reduced by two orders of magnitude by changing the estimate of gamma from 0.01 to 1, a not unreasonable difference. It can further be reduced by assuming a non-isotropic distribution of atoms. (What shape distribution should be used, however, is dependent on the formation mechanism of the high speed molecules.)

II. ION EMISSION

The work on ion emission for this period has been concentrated primarily on the interpretation of the pulse shapes. On the experimental side we have obtained photographs of pulses with enough time resolution to be useful in the analysis. We have also measured the dependence of the time of flight of several mass peaks on the accelerating potential used in the TOF spectrometer[1]. These results and their use in finding the velocity distribution of the ions are presented in this section. The interpretation of data is presented in Section III.

The ion emission from a thin platinum target was also measured. The results seem to indicate that the mechanism of ion acceleration involves a direct interaction of the emitted gas with the laser beam. The emission itself is qualitatively similar to that of tungsten.

A. ION EMISSION FROM PLATINUM

The purpose of measuring ion emission from platinum is twofold: First, it provides us with a different surface to compare with tungsten; second, it allows us to check on whether or not the laser beam is directly involved in the formation of the ions observed.

Figure II-1 shows a typical spectrum obtained from platinum when irradiated on the surface facing the spectrometer. The spectrum is similar to that obtained from tungsten surfaces in that the major peaks are still Na^+ and K^+. Other peaks are present but they are much smaller. On the other hand, while K^+ is the largest peak in the emission from tungsten, the Na^+ peak is largest for platinum. The ion energies from both surfaces are similar for equivalent laser outputs. In general the emission from the two surfaces (platinum and tungsten) is quite similar except for the relative abundances of different species.
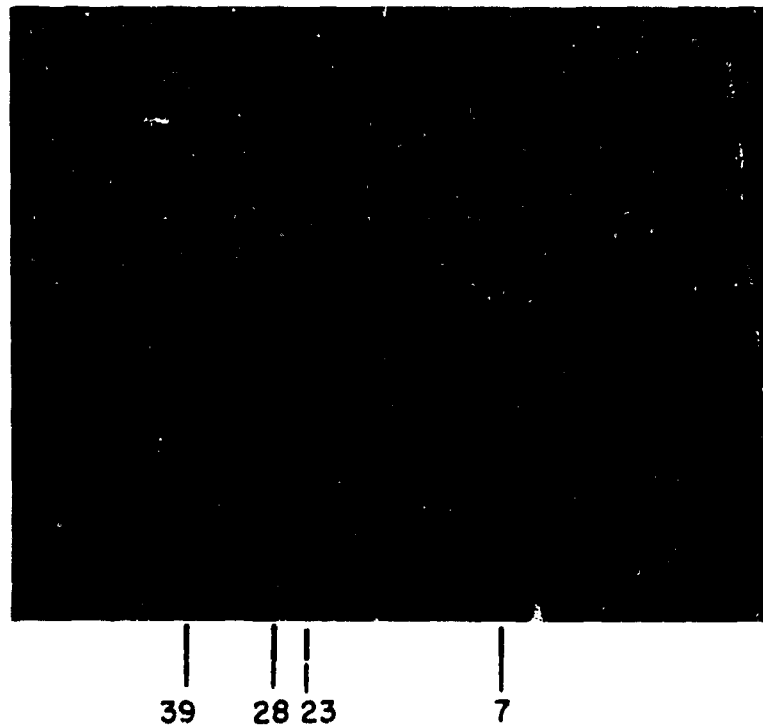
Figure II-1 - Typical Mass Spectrum from Platinum Target in TOF Spectrometer. Time increases from right to left. Lower trace starts with laser pulse (2 μs/cm, .1 v/cm). Upper trace is an expanded portion of the lower trace triggered by the mass 23 pulse (.5μ sec/cm, .05 v/cm.) The spectrometer potentials are: V = +1000v.; v' = +1022v.

The platinum target used in these experiments was 5 microns thick. Calculation of the bulk temperature upon irradiation shows that the temperature gradient is negligible across the thickness of the target. Hence, if the mechanism for ion production and acceleration did not involve a direct interaction with the laser beam, one should obtain essentially the same ion emission regardless of which side of the target was irradiated.

The results obtained from irradiation of the back side of the target were all negative. The absence of ions was observed in experiments that consisted of alternating the laser beam between the front and back surfaces, with emission observed always from the front surface. These results are consistent with the hypothesis that the creation and acceleration of ions is associated with a direct interaction with the laser beam and is inconsistent with the hypothesis that ions are produced by a shock wave traversing the target.

B.   ELECTRIC FIELD DEPENDENCE OF TIME OF FLIGHT

The time of flight was measured as a function of field for the major ion peak of tungsten and platinum surfaces. This information is important in determining the validity of mass assignments which are based on calculations that assume independent particle behavior of the emission from the metal. In the analysis of pulse shapes to arrive at a velocity distribution (which is discussed later in this report), it is assumed that the time of flight can be written as

$$t = \frac{\ell}{v_d(w)} \tag{II-1}$$

where ℓ = effective length of drift region, and

$$v_d(w) = \sqrt{\frac{2e}{m}\left[V(x_d) - V(o)\right] + w^2} \tag{II-2}$$

-22-

is the velocity in the drift tube of singly charged ions of mass m with initial velocity w and accelerated by a potential difference $V(x_d) - V(o)$. The above expression involve two assumptions: first, that the time spent outside of the drift tube is small compared to the drift time; second, that the particles emitted by the target behave as independent particles in their reaction to externally applied fields.

The last assumption is particularly crucial not only for the analysis of distributions, but also to test the validity of our conclusions regarding ion masses. We have therefore measured the time of flight as a function of applied field. If the above assumptions are justified, we can combine Equations (II-1) and (II-2) to obtain

$$ t^{-2} = \frac{2e}{m\ell^2} \left[V(x_d) - V(o) \right] + \left(\frac{w}{\ell} \right)^2 . \qquad \text{(II-3)} $$

Figures II-2 and II-3 show the measured arrival times as a function of applied voltage for the largest mass peaks obtained from tungsten and platinum; they correspond to masses 39 and 23 respectively. The points represent the measured values and the curves represent the best fit to the data in the least squares sense.

It can be seen that the data fits the straight line predicted by Equation II-3 quite well. We take this to be evidence of the fact that the plasma consisting of the particles emitted by the target is very short lived; i.e., macroscopic charge neutrality is not maintained over distances comparable to the dimensions of the accelerating gap. This measurement, therefore, is another piece of evidence which justifies the assignment of ion masses on the basis of the times of flight measured in the spectrometer.
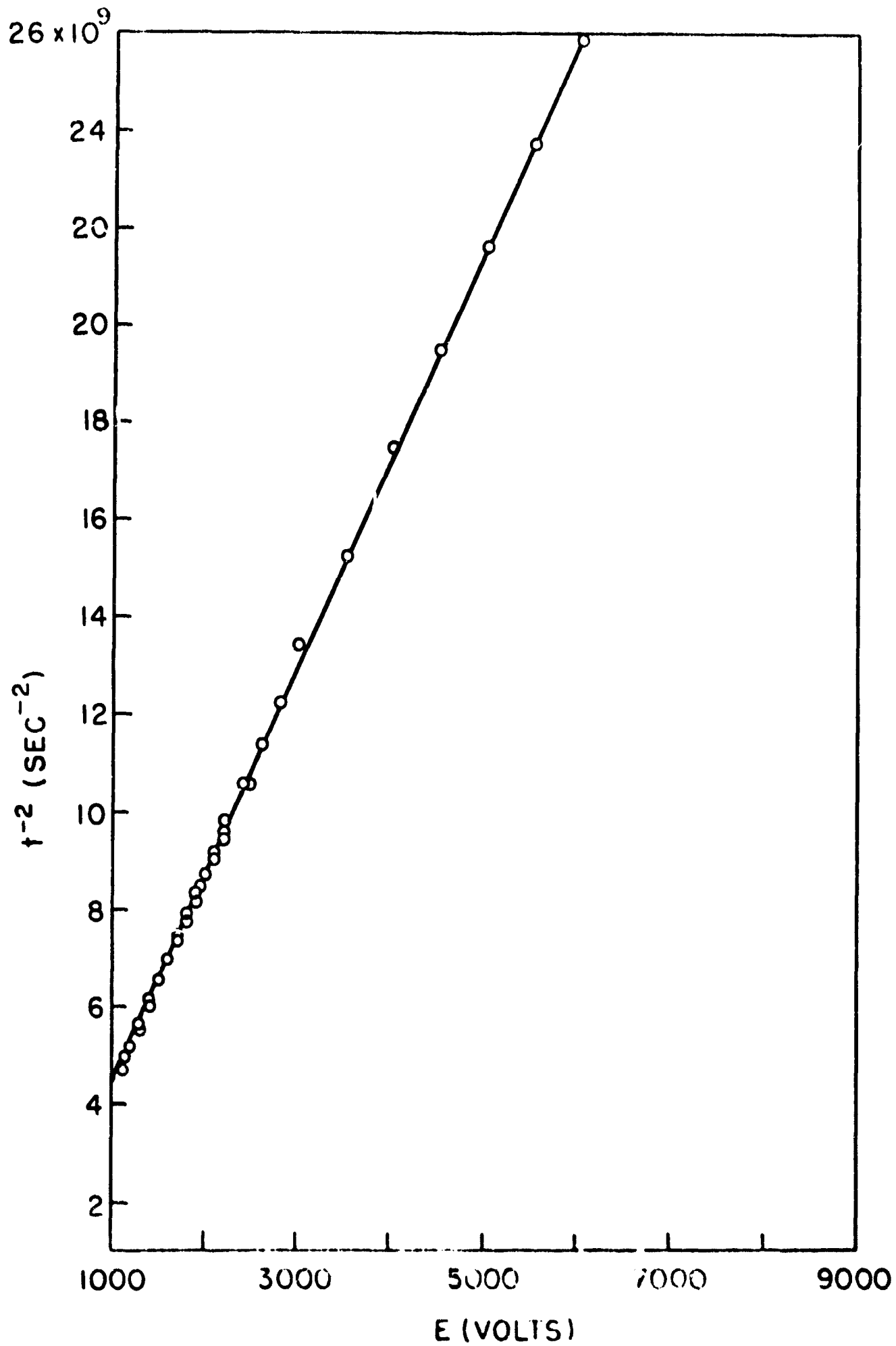
Figure II-2 - Time of Flight vs. Accelerating Potential for the K^+ (39) Peak from Tungsten Target

-24-
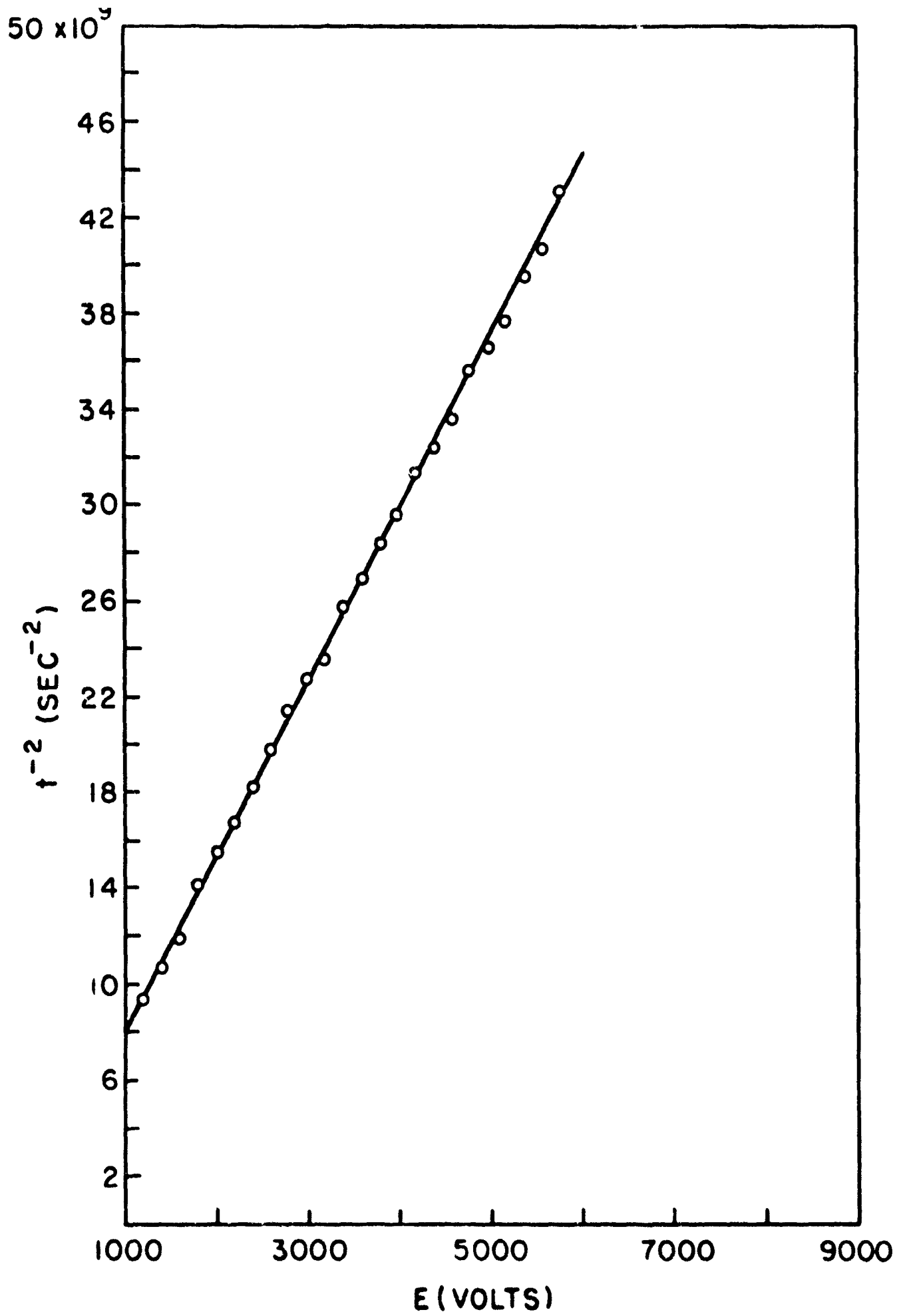
Figure II-2 - Time of Flight vs. Accelerating Potential for the Na$^+$ (23) Peak from Platinum Target

One further question that must be answered before proceeding with the analysis of the measured pulse shapes is: What is the effective length ℓ that should be used in calculating t in Equation (II-1)? Neglecting initial ion energies as compared to those given by the fields, it is easy to show that the effective "drift length" of the spectrometer is ~ 105 cm. The argument is as follows: Let $\ddot{x} = a$ in the accelerating gap and $v_d(w)$ be the velocity at the end of the gap (entrance to drift tube); w is the initial particle velocity. Then,

$$v(w) = at + w.$$

If we let t_d be the time required to cross the gap,

$$v_d(w) = at_d + w$$

$$\bar{v}(w) = \frac{1}{t_d} \int_0^{t_d} v(w)dt = \frac{1}{2} a t_d + w$$

and

$$x_d = \frac{1}{2} a t_d^2 + wt_d = \bar{v}(w)t_d \qquad (II-4)$$

We assume that $at_d \gg w$; i.e., the energies supplied by external fields are much larger than the initial energies. Then

$$v_d \cong 2\bar{v} \qquad (II-5)$$

Using (II-5) in (II-4), we obtain

$$2x_d = v_d t_d . \qquad (II-6)$$

Hence, since we wish to treat the spectrometer as if the particles had a constant velocity v_d while traversing it, (II-6) gives the prescription for handling the regions where fields are applied. For the particular field configurations used in the spectrometer[1], equation (II-6) says that we must double the actual length of the region. Using this prescription we obtain an effective drift length $\ell \sim 105$ cm.

With the drift length we can now check the mass assignments of the peaks of Figures II-2 and II-3. The slopes corresponding to the least squares fit are $4.7 \times 10^{+6}$ for the peak from tungsten and $7.8 \times 10^{+6}$ for the peak from platinum. The slopes calculated for masses 39 and 23 using Equation (II-3) are $4.65 \times 10^{+6}$ and $7.89 \times 10^{+6}$ respectively. The agreement between the experimental and calculated values is another confirmation of the correctness of mass assignments.

C. EXTENSION OF PULSE SHAPE ANALYSIS

In the last semi-annual report,[1] it was shown that for a monoenergetic pulse of ions of a given shape, the detector signal in the time-of-flight spectrometer would reproduce the shape of the pulse. In this report we extend the proof to any parallel-plate structure and to an arbitrary pulse shape. The one-dimensional equation of continuity

$$\frac{\partial J}{\partial x} + \frac{1}{v} \frac{\partial J}{\partial t} = 0$$

governs the flow of charge in the spectrometer. Its Laplace transform is[5]

$$\frac{dj}{dx} + \frac{s}{v} j = 0 \tag{II-7}$$

-27-

Equation (II-7) has a solution

$$j(x,s) = j(o,s) \exp\left[-s\int \frac{dx}{v}\right] = L[J(x,t)] \tag{II-8}$$

where $\quad j(o,s) \quad L[J(o,t)]$, $\tag{II-9}$

i.e., $j(o,s)$ is the Laplace transform of the boundary conditions. In general, v may or may not be constant, depending on whether or not external fields are present. However, it is a well known property of Laplace transforms that if (II-9) is true, then[5]

$$j(o,s) \exp\left[-s\int \frac{dx}{v}\right] = L\left[J(o, t - \int \frac{dx}{v})\right] \tag{II-10}$$

Comparing (II-8) and (II-10), we find that for an arbitrary parallel-electrode geometry, or for that matter any structure for which $\frac{\partial v}{\partial t} = 0$, the convection current at any point is simply the current at the target delayed by the time of flight from target to detector. Notice that the proof is independent of any assumptions about pulse shapes.

The above proof suggests a possible new structure that can be used to obtain information on both the density $\rho(o, w, t)$ at the target and the initial ion velocity w. Consider a triode consisting of a target, an accelerating grid followed by a drift region, and a collector. Using the results of the last semi-annual report[1], one finds that if the detector is a plain electrode, then the detector current I satisfies

$$\frac{dI}{dt} = \frac{wA}{d} J(o,t) \tag{II-11}$$

where w = initial ion velocity

  A = detector area

  d = separation between accelerating grid and detector.

On the other hand, if one uses an electron multiplier detector, the current is given by

$$I(t) = gA \, J(o, t); \quad g = \text{multiplier gain.} \tag{II-12}$$

The above arrangement can be used as follows: If a target emitting particles of only one mass is used, the ratio of the two signals given by (II-11) and (II-12) gives the initial ion velocity w as a function of time. The two signals can be derived from different electrodes in a two stage multiplier detector. Knowledge of w allows one to compute the ion density. In practice the emission is not monoenergetic, and it would be necessary to bias the detector to admit only a small range of velocities. The single mass requirement may possibly be satisfied either by using laser powers that are high enough to evaporate a considerable amount of the target material per shot, or by using a (100) face of single crystal nickel that can be covered with hydrogen exclusively.

III. INTERPRETATION OF DATA

This portion of the report covers the interpretation of the experimental results
described in the previous two sections. It includes the work that is basically
theoretical or computational. There are three main topics considered in this
section: The first involves processing the measured pulse shapes of emitted
particles to infer their original velocity spectrum. The second involves
extensions of work described in the semi-annual report[1]; namely, the cal-
culation of the heating effects that arise from absorption of the laser light
by free-free transitions in the blow off material. The third is a discussion of
the identification of the masses and energies of the neutral particles described
in Section I. While the identification is not definite, some tentative hypotheses
are made.

A. DETERMINATION OF VELOCITY DISTRIBUTION

The calculation of the ion velocity distribution from the measured pulse
shapes is based on the analysis given in Appendix I. We will review briefly
here those parts that are relevant to this discussion and indicate how the
data is processed. Basically we assume that the ion pulse from the target
is a δ-function in time, i.e., we assume that the finite width of the pulse at
the detector is due to a distribution in initial ion velocities. This
assumption is justified on the basis that the width of the ion pulse at the
detector is much longer than that of the laser pulse during which one would
expect the ion emission to occur. The above assumption establishes a
one-to-one correspondence between time of arrival and initial ion velocity with the
time of arrival of zero velocity ions corresponding to the end of the detector
pulse.

Now, the velocity $v_d(w)$ of a singly charged ion of mass m with initial
velocity w, accelerated through a potential difference $V(x_d)-V(o)$, is

$$v_d(w) = \sqrt{\frac{2e}{m} \left[V(x_d) - V(o) \right] + w^2} \qquad \text{(III-1)}$$

Furthermore, since most of the time of flight t is spent in the drift tube, we approximate it by

$$t = \frac{\ell}{v_d(w)} \qquad \text{(III-2)}$$

where ℓ is an effective drift length that corrects for time spent outside the drift tube. The justification for this approximation was given in Section II-B. Notice that (III-2) implies the δ-function assumption for the emission pulse. From (III-1) and (III-2) we get

$$\frac{dt}{dw} = \frac{\ell w}{v_d^3(w)} \qquad \text{(III-3)}$$

Now, if we let N(w) represent the distribution of velocities of the ions at the target, conservation of charge requires that

$$k \int_0^\infty N(w)\,dw = \int_0^\infty J(t)\,dt \qquad \text{(III-4)}$$

where J(t) is the signal from the detector; k is the constant transmission coefficient of the spectrometer. We can rewrite (III-4) as

$$\int_0^\infty \left[kN(w) - J(t)\,\frac{dt}{dw} \right] dw = 0$$

from which we find the prescription for calculating N(w),

$$N(w) = k^{-1} J(t)\,\frac{dt}{dw} . \qquad \text{(III-5)}$$

The application of the above to the data is as follows: Values of $J(t)$ measured at equal intervals are stored in a computer. The end of the pulse is taken to be the time of arrival of the ions with zero initial velocity ($w = 0$). A constant initial velocity increment dw is chosen and added to w. With the new w used in (III-1), (III-2) and (III-3), new values of t and dt/dw are calculated. These values are then used to calculate $N(w)$ using (III-5) and values of $J(t)$ interpolated from the data stored in the computer. The process continues with a new increment dw. At each step the quantities $wN(w)$ and $w^2N(w)$ are calculated and stored cumulatively to calculate the average velocity w of the center of mass, as well as the random energy about the center of mass. The average velocity is calculated from Equation (19a) of Appendix I:

$$\bar{w} = \frac{\Sigma \, wN(w) \, dw}{N} \tag{III-6}$$

where $N = \Sigma \, N(w) \, dw$. The random energy of Equation (19b) of the Appendix is calculated using the following simplification:

$$\frac{1}{N} \Sigma (w - \bar{w})^2 \, N(w) \, dw = \frac{1}{N} \Sigma \, (w^2 - 2w \, \bar{w} + (\bar{w})^2) \, N(w) \, dw = \frac{1}{N} \Sigma w^2 N(w) \, dw - (\bar{w})^2$$

Using the above method one eliminates the need to calculate $\bar{w}$ first, and then repeat the calculation to form $(w - \bar{w})^2$ at each stage.

A sample of the computer output of a typical calculation, corresponding to the results shown in Figure III-3 is given in Table III-1.

A word of caution seems in order at this point. While the calculations described above are straightforward, it is important to choose a small value of the velocity increment dw. If dw is too large, the measured pulse shape $J(t)$ changes drastically during the corresponding time increment dt, and the resulting velocity distribution appears deceivingly symmetrical. In fact, in some of our earlier calculations of velocity distributions, the results looked like a good fit to a Maxwellian because of this effect.

TABLE III-1

TYPICAL CALCULATION OF N(w) FROM MEASURED PULSE SHAPE J(t)

W	T	J (T)	N (W)
+0.000E-99	+8.2081E-06		
+1.00E+05	+8.2078E-06	+1.6155E-03	+8.1490E-18
+2.00E+05	+8.2071E-06	+6.4611E-03	+6.5165E-17
+3.00E+05	+8.2058E-06	+1.4534E-02	+2.1978E-16
+4.00E+05	+8.2041E-06	+2.5830E-02	+5.2046E-16
+5.00E+05	+8.2018E-06	+4.0343E-02	+1.0152E-15
+6.00E+05	+8.1990E-06	+5.6064E-02	+1.7517E-15
+7.00E+05	+8.1958E-06	+7.8985E-02	+2.7766E-15
+8.00E+05	+8.1920E-06	+1.0309E-01	+4.1362E-15
+9.00E+05	+8.1877E-06	+1.3037E-01	+5.8755E-15
+1.00E+06	+8.1830E-06	+1.6081E-01	+8.0386E-15
+1.10E+06	+8.1777E-06	+1.9440E-01	+1.0668E-14
+1.20E+06	+8.1720E-06	+2.3111E-01	+1.3807E-14
+1.30E+06	+8.1658E-06	+2.7092E-01	+1.7494E-14
+1.40E+06	+8.1591E-06	+3.1382E-01	+2.1769E-14
+1.50E+06	+8.1519E-06	+3.5838E-01	+2.6566E-14
+1.60E+06	+8.1443E-06	+4.0037E-01	+3.1568E-14
+1.70E+06	+8.1361E-06	+4.4495E-01	+3.7164E-14
+1.80E+06	+8.1276E-06	+4.9207E-01	+4.3381E-14
+1.90E+06	+8.1185E-06	+5.4174E-01	+5.0244E-14
+2.00E+06	+8.1090E-06	+5.9390E-01	+5.7778E-14
+2.10E+06	+8.0991E-06	+6.4855E-01	+6.6005E-14
+2.20E+06	+8.0887E-06	+6.8709E-01	+7.2976E-14
+2.30E+06	+8.0778E-06	+7.2677E-01	+8.0375E-14
+2.40E+06	+8.0665E-06	+7.6804E-01	+8.8262E-14
+2.50E+06	+8.0548E-06	+8.1088E-01	+9.6646E-14
+2.60E+06	+8.0427E-06	+8.6188E-01	+1.0635E-13
+2.70E+06	+8.0302E-06	+9.6520E-01	+1.2310E-13
+2.80E+06	+8.0172E-06	+1.0719E+00	+1.4109E-13
+2.90E+06	+8.0038E-06	+1.1819E+00	+1.6033E-13
+3.00E+06	+7.9901E-06	+1.2953E+00	+1.8082E-13
+3.10E+06	+7.9759E-06	+1.7226E+00	+2.4718E-13
+3.20E+06	+7.9614E-06	+2.1750E+00	+3.2040E-13
+3.30E+06	+7.9465E-06	+2.6391E+00	+3.9867E-13
+3.40E+06	+7.9312E-06	+3.1553E+00	+4.8826E-13
+3.50E+06	+7.9155E-06	+3.8143E+00	+6.0400E-13
+3.60E+06	+7.8995E-06	+4.4882E+00	+7.2660E-13
+3.70E+06	+7.8831E-06	+5.1769E+00	+8.5603E-13
+3.80E+06	+7.8664E-06	+6.6116E+00	+1.1156E-12
+3.90E+06	+7.8494E-06	+8.2332E+00	+1.4166E-12
+4.00E+06	+7.8320E-06	+9.8860E+00	+1.7330E-12
+4.10E+06	+7.8143E-06	+1.0335E+01	+1.8446E-12
+4.20E+06	+7.7963E-06	+1.0071E+01	+1.8287E-12
+4.30E+06	+7.7780E-06	+9.8038E+00	+1.8096E-12
+4.40E+06	+7.7594E-06	+8.8153E+00	+1.6530E-12
+4.50E+06	+7.7405E-06	+7.3629E+00	+1.4018E-12
+4.60E+06	+7.7213E-06	+5.8888E+00	+1.1375E-12
+4.70E+06	+7.7019E-06	+4.0512E+00	+7.9358E-13
+4.80E+06	+7.6822E-06	+2.0663E+00	+4.1020E-13
+4.90E+06	+7.6622E-06	+5.5237E-02	+1.1107E-14
+5.00E+06	+7.6420E-06	+0.0000E-99	+0.0000E-99

$$\overline{N} \qquad +2.02477652E-06$$
$$\overline{W} \qquad +3.97315953E+06$$
$$\overline{(W-\overline{W})^2} \qquad +3.54304060E+11$$

1. Ion Velocity Distribution

Several of the expanded photographs of mass peaks obtained in the TOF spectrometer have been subjected to the analysis described above in an attempt to find the velocity distribution of the ions. Before analyzing the data, we determined experimentally that the time of flight can be reasonably approximated by an expression such as Equation (III-2), and determined an effective length to be used in that equation. Those results are reported in Section II. Figure III-1 shows mass pulses obtained from a tungsten target. From left to right they correspond to masses 23 and 39 respectively. The accelerating potential applied to the target was $V = +2000$ volts. The velocity distribution obtained from the analysis of the mass pulses are given in Figures III-2 and III-3 for the mass 39 and mass 23 peaks respectively. The mass 39 pulse has a center of mass velocity, $\bar{w} = 3.2 \times 10^6$ cm/sec, corresponding to a directed energy of the center of mass of 207 ev. The random energy, assuming equipartition, is 16 ev. The corresponding parameters for the mass 23 pulse are $\bar{w} = 4.0 \times 10^6$ cm/sec, directed center of mass energy of 190 ev, and random energy of 13 ev. In both Figures III-2 and III-3 we have plotted the Maxwellian distribution

$$N_m(w) = N\left(\frac{m}{2\pi k T}\right)^{1/2} \exp\left[-\frac{m}{2kT}(w - \bar{w})^2\right]$$

with N, w and T taken from the calculated distributions.

Qualitatively it appears that the calculated velocity distributions of Figures III-2 and III-3 do not fit a Maxwellian well, for they are asymmetric and obviously peaked at high velocities. Also, the maximum energies of the ions in the calculated distributions are 312 ev for the mass 39 pulse and 288 ev for the mass 23 pulse. These energies are about 100 ev higher than the measured ion energies.

$$\underset{\overset{|}{K^+}}{} \quad \underset{\overset{|}{Na^+}}{}$$

Figure III-1 - Na^+ and K^+ Pulses from Tungsten Target with an Accelerating Potential of +2000v. Time increases to left. Lower trace triggers with laser pulse and sweeps at 2 μsec/cm. Upper trace triggers on Na^+ peak and sweeps at 0.5 μs/cm.
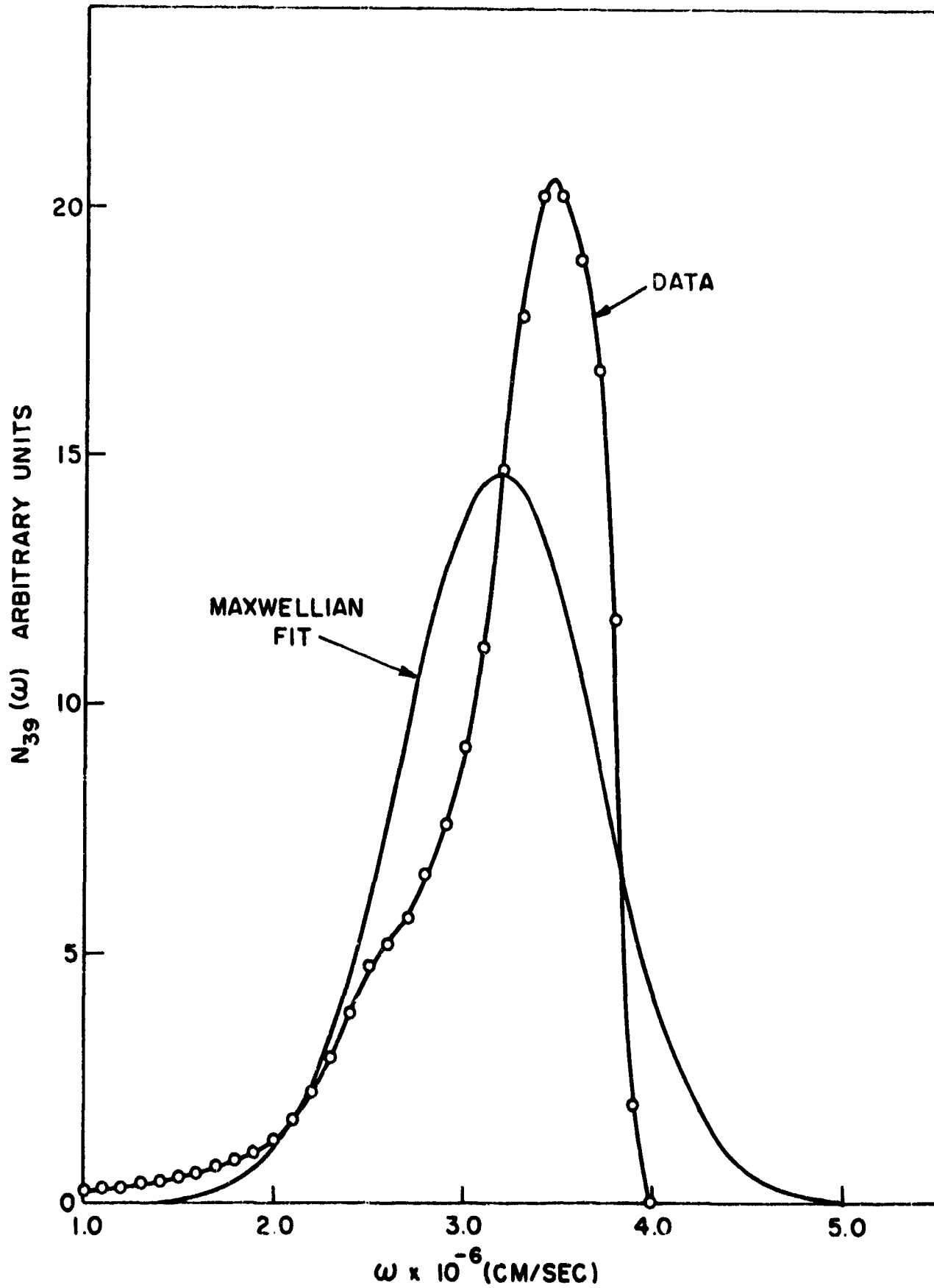
Figure III-2 - K^+_{39} Velocity Distribution $N_{39}(w)$ Calculated from Data of Figure III-1. Maxwellian Fit Included for Comparison.

-36-
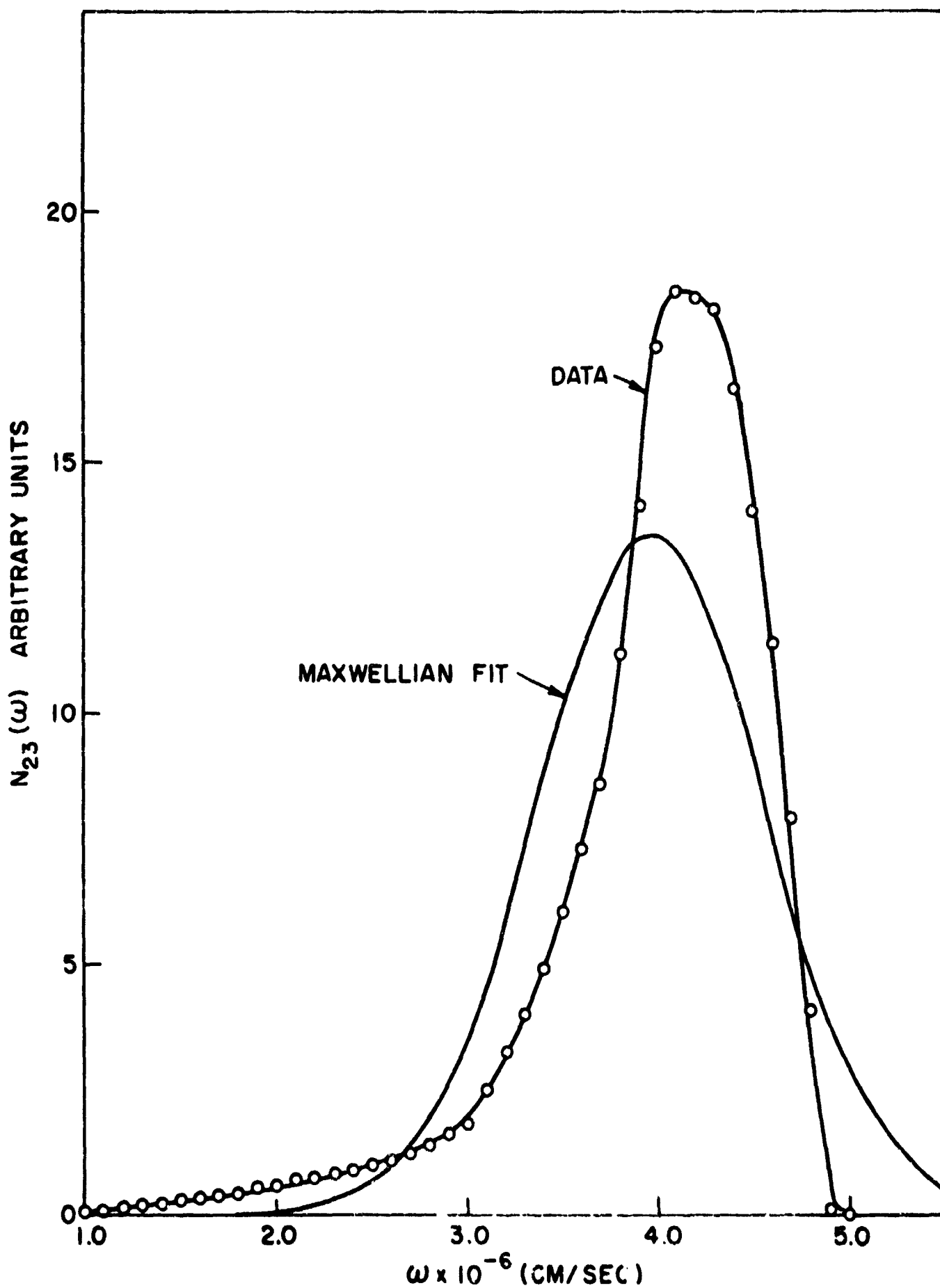
Figure III-3 - Na^+_{23} Velocity Distribution $N_{23}(w)$ Calculated from Data of Figure III-1. Maxwellian Fit Included for Comparison.

A more careful examination of the facts, however, suggests that the agreement may be better than it appears: First, the distributions correctly predict that the ions in the mass 39 pulse are more energetic than those of the mass 23 pulse, and predicts a difference of ~ 30 ev for the maximum energies. This is in agreement with measurements. Second, if we assume that the emission of ions lasts for 200 nanoseconds, not an unreasonable length of time, we find that the corresponding maximum energies of the two pulses in question become 225 and 188 ev respectively, in good agreement with the measured values of ion energies and still preserving the proper difference in energy between the two. Third, if a finite pulse width of 200 nanoseconds is assumed, it is possible that a superposition of Maxwellians for that time interval would lead to measured distributions such as those of Figures III-2 and III-3. Some attempts have been made to simulate such finite pulses numerically, as reported in III A 3; however, more work needs to be done in that area because there are many adjustable parameters.

In conclusion, we note that the ion energies for different species emitted from a given target are approximately the same, but not exactly equal. From results obtained so far, it appears that there are differences between the velocity distributions and Maxwellian distributions.

2. Velocity Spectrum of Neutral Molecule Pulses

The analysis of the velocity distribution can also be applied to the neutral particle pulses described in Section I to determine their initial energy distribution. This application involves more uncertainties than in the case of the ions in the time of-flight instrument since the particle identities are not certain.

Let us carry through the analysis on a pulse that appears typical. The pulse analyzed is shown in Figure III 4. This data was obtained with a tungsten target and a laser power of about 60 megawatts/cm^2. There are two different particle pulses. This result is typical of the data obtained with tungsten targets.

These pulses were analyzed according to the method described earlier. The resulting velocity spectra are shown in Figures III 5 and III 6. Also shown in each figure is the Maxwellian distribution for the same average velocity, and normalized to the same number of particles as the experimental $N(w)$. The results of Figure III 5 are very similar to those described above in the analysis of the ion pulses. The velocity distribution appears to consist of a directed component and a random component. As before, the Maxwellian is not a good fit. The observed curve has a peak at higher value than w, and falls off more rapidly on the high velocity end. Near the wings, as the distribution approaches zero, the observed distribution falls below the Maxwellian. The appearance of the peak at a velocity larger than w is similar to the result obtained with the ion pulses. We do not expect the distribution to go to zero as the ions did since the efficiency γ is zero at $w = 0$.

In deriving these distributions, we have neglected the fact that the efficiency γ, with which a high velocity atom produces electrons at the cathode of the multiplier, is a function of energy. Little data on this efficiency is available but some estimates of its possible behavior are made in Section I. If the efficiency varies as a function of atom velocity over the range of interest, it means that the curves presented here should be modified by a factor containing the efficiency γ. In particular, if γ increases with increasing velocity of the incident particle, the low energy portion of the distribution should be increased relative to the high energy portion. We intend to investigate this factor further.
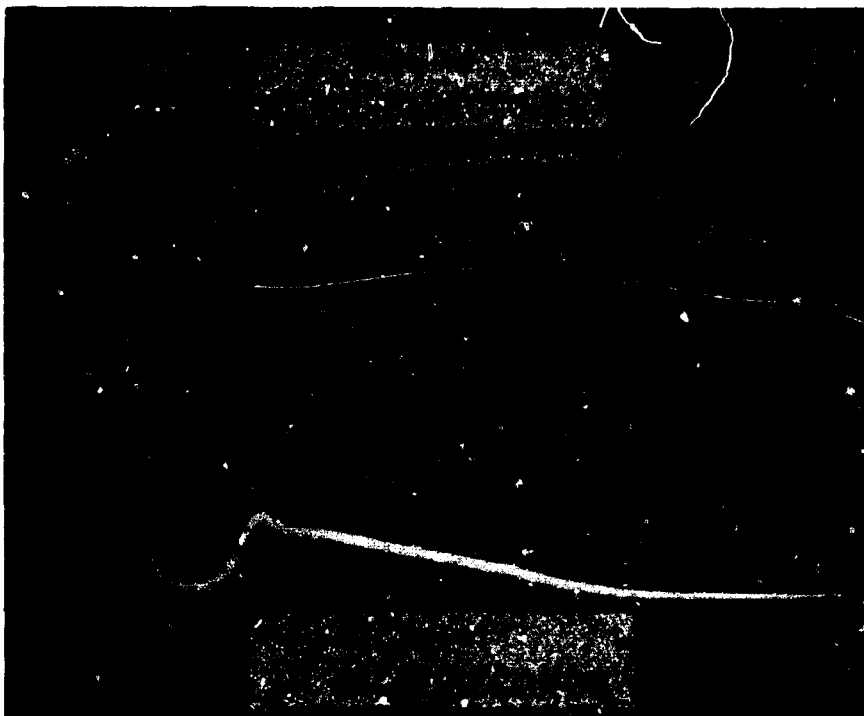
Figure III-4 - Typical High Speed Molecule Pulse Obtained by Irradiation
of Tungsten Target with Laser Pulse of 60 Mw/cm^2. Time increases from
left to right.
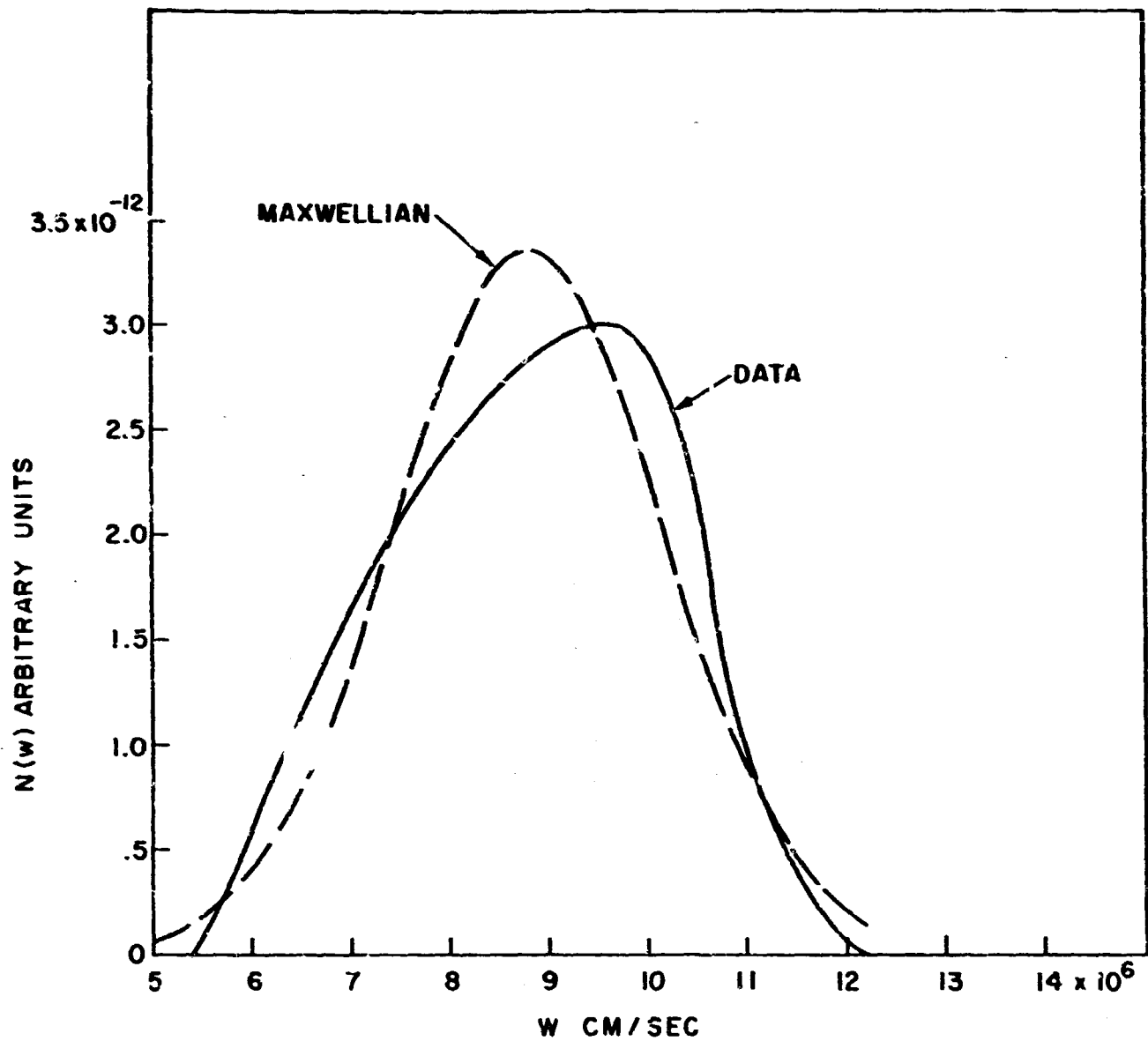
Figure III-5 — Velocity Distribution N (w) Calculated from First Neutral Particle Pulse of Figure III-4. Maxwellian Fit Included for Comparison.
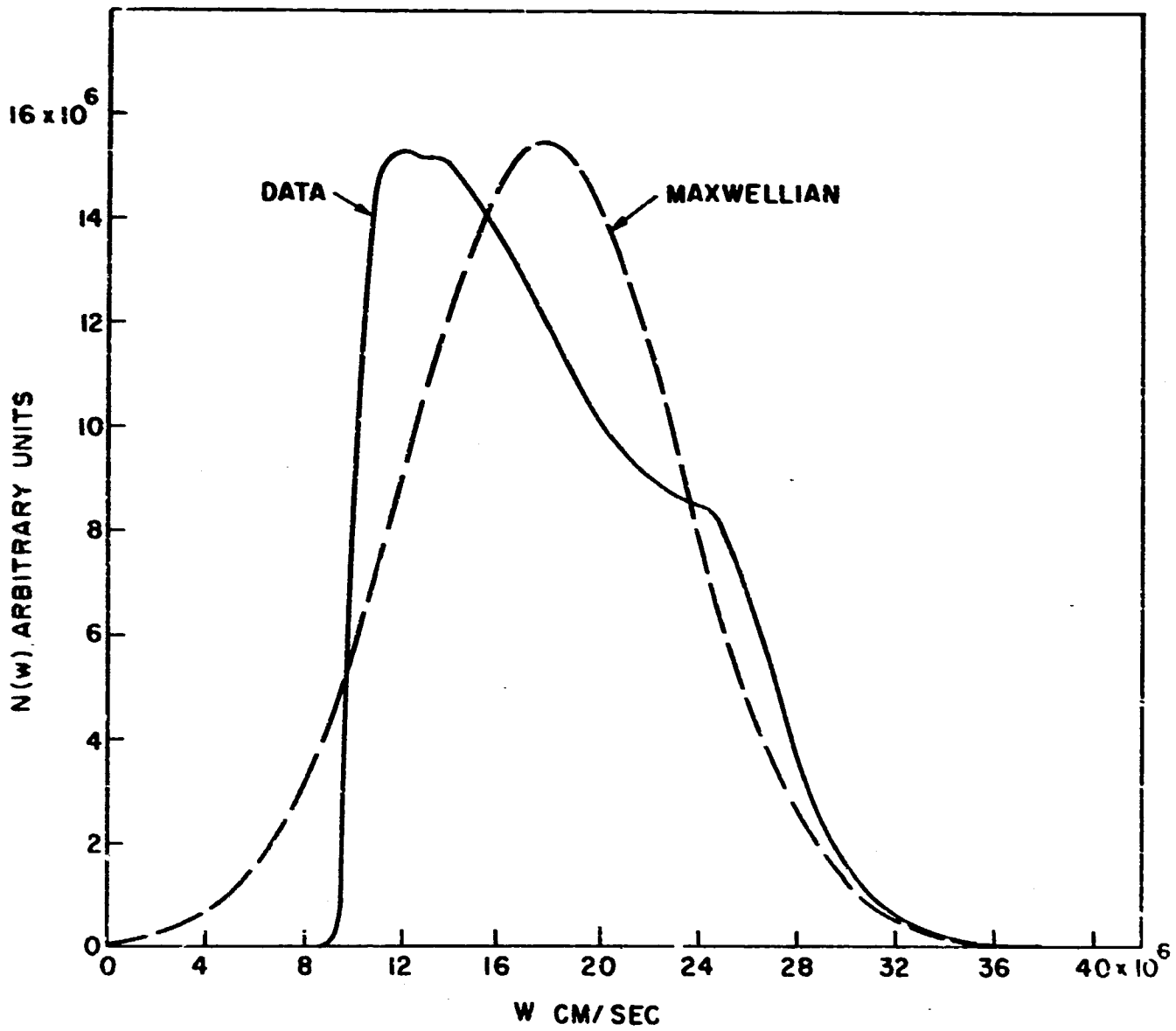
Figure III-6 - Velocity Distribution N (w) Calculated from Second Neutral
Particle Pulse of Figure III-4. Maxwellian Fit Included for Comparison.

Since the natures of the particles are not known yet, we give the results for the energy distributions in terms of the atomic number A of the particle. For the first molecule pulse in Figure III-4, we find:

Center of Mass Energy in ev $= 39.0 \times A$

Random Energy - one component - in ev $= 0.91 \times A$

Random Energy - three components - in ev $= 2.7 \times A$

For the second neutral molecule pulse in Figure III-4 we find:

Center of Mass Energy in ev $= 1.57 \times A$

Random Energy - three components - in ev $0.45 \times A$

If the atomic number A of the particle were known, the energy would be known; e.g., if the first pulse has $A = 2$ (molecular hydrogen), we would obtain 78 ev for the center of mass energy and 5.4 ev for the random energy.

We should note that this is one sample which we have described in detail here. Other pulses have been analyzed and yield similar results both for the shape of the distribution and the energy.

These results will be used below in Section III-C where we will attempt to deduce the nature of these atom pulses. The conclusions of this subsection are that the same analysis that was applied to the ion pulse shapes may be applied to the neutral atom pulse shapes. The results indicate a large directed energy component with a smaller random component. The velocity distributions differ somewhat from a Maxwellian. In these respects the results are similar to those obtained in the analysis of the ion pulses. The magnitudes of the energy components cannot be deduced here because of uncertainty about the nature of the particles, but only the ratio of energy to atomic number.

3. Calculation of Pulse Shapes From Inferred Velocity Distributions

This subsection has to do with an attempt to remove the δ function assumption in the analysis described in Sections IIIA1 and IIIA2. In Appendix 1 it is suggested that the shape of the pulse J (t) be calculated using the assumptions of a square emission pulse in time and a Maxwellian distribution for the velocity. This procedure involves evaluating the integral in Equation (23) of Appendix I. As is pointed out there, even with these fairly restrictive assumptions, the integral cannot be evaluated analytically.

Accordingly a computer program was written to evaluate this integral numerically. The case chosen was that of mass 39 ions with a 1000 volt accelerating potential. The shape of the pulse was calculated by evaluating the integral using Equation (23) described in Appendix I. The function c, defined in Appendix I as the density of ions per unit initial speed w in the x direction, is given for a Maxwellian by:

$$c\ (o,\ w,\ t) \ = \ F(t)\ \exp\ -\ \left[\frac{m(w-\bar{w})^2}{2kT(t)} \right] \tag{III-7}$$

Here $\bar{w}$ is the average velocity of the distribution, corresponding to the directed energy component; it is assigned as an independent variable so that the peak of the pulse occurs at the same time as that experimentally observed. The following assumptions are made: (1) The random component is a Maxwellian characterized by a temperature; (2) the temperature is a given function of time; (3) The function $F(t)$ gives the shape of the emission pulse and is also known. Table III-2 lists the various cases which were calculated. Equation (23) strictly applies only to those cases in which the emission pulse is flat and the temperature is constant. Expressions somewhat different from the integral in Equation (23) must be evaluated for the cases in the table which do not comply with these restrictions.

-44-

SETS OF EMISSION PULSE PARAMETERS USED IN THE INTEGRATION OF EQUATION (23) OF APPENDIX I.

CASE	$\bar{W}$ $(10^6 CM/SEC)$	F (t)		T (t)	
		DURATION OF PULSE (NS)	SHAPE OF PULSE	SHAPE	PEAK TEMPERATURE $^\circ K$
1	2.5	200	FLAT	FLAT	10^5
2	2.5	200	FLAT	FLAT	2×10^5
3	4.0	200	FLAT	FLAT	10^6
4	4.0	200	FLAT	FLAT	10^5
5	3.0	200	FLAT	FLAT	10^5
6	3.0	200	TRIANGULAR (PEAK AT 0)	FLAT	10^5
7	3.0	200	TRIANGULAR (PEAK AT 0)	FLAT	2×10^5
8	3.0	200	FLAT	FLAT	2×10^5
9	2.5	100	FLAT	FLAT	10^5
10	2.5	200	FLAT	FLAT	3×10^5
11	2.5	200	FLAT	FLAT	6×10^5
12	2.5	200	FLAT	FLAT	12×10^5
13	3.5	200	FLAT	FLAT	10^4
14	3.5	200	FLAT	FLAT	10^5
15	3.5	200	TRIANGULAR (PEAK AT 0)	FLAT	10^5
16	3.5	100	FLAT	FLAT	10^5
17	3.5	50	FLAT	FLAT	10^5
18	3.5	100	FLAT	FLAT	2×10^5
19	3.5	200	FLAT	FLAT	2×10^5
20	3.5	200	FLAT	TRIANGULAR (PEAK AT 0)	10^5
21	3.5	1000	FLAT	FLAT	10^5
22	3.5	1000	TRIANGULAR (PEAK AT 0)	FLAT	10^5
23	3.5	1000	TRIANGULAR (PEAK AT 0)	FLAT	5×10^4
24	3.5	1000	TRIANGULAR (PEAK AT 0)	TRIANGULAR (PEAK AT 0)	10^5
25	3.5	1000	FLAT	TRIANGULAR (PEAK AT 0)	10^5

This computation essentially does in reverse the analysis done in Sections IIIA2 and IIIA3. There we started with an observed pulse shape and obtained a velocity distribution. Now we start with an assumed velocity distribution and calculate a pulse shape.

We find that a choice of $\bar{w} = 3.5 \times 10^6$ cm/sec gives the best fit for the peak of the calculated data as compared to the experimentally observed pulses. Most of the cases in Table III-2 were run with this value of $\bar{w}$.

From the computer runs, we found that the calculated pulse shapes could not be varied appreciably by any of the choices of parameters listed in Table III-2. As was pointed out before, care must be exercised in choosing the mesh size for the numerical integration. The first few runs on the computer were made using too large a mesh which gave spurious results indicating considerable changes of the pulse shape with the variable parameters. Later work with a smaller mesh is described in this report.

Some of the results of the computer runs are presented in Figures III-7, 8, 9 and 10. In these figures the calculated pulse shapes are shown for several of the cases listed in Table III-2, all of them with $\bar{w} = 3.5 \times 10^6$ cm/sec. The vertical scales are in arbitrary units; they are not even the same scale for all cases. The important consideration is the relative shape of the pulses; e. g., the time of the peak, the width, the relative slope of the rising and decaying portions.

In Figure III-7 we see the effect of changing the duration of the emission F(t) from 50 to 1000 nanosecond, with F(t) assumed flat for all the cases. As the length of F(t) increases, the width of J(t) increases, as we would expect, and the peak value of J(t) comes later, as we also expect. However, the shape of the pulse J(t) does not change dramatically it remains roughly a symmetrical triangular pulse. If the velocity distribution obtained in
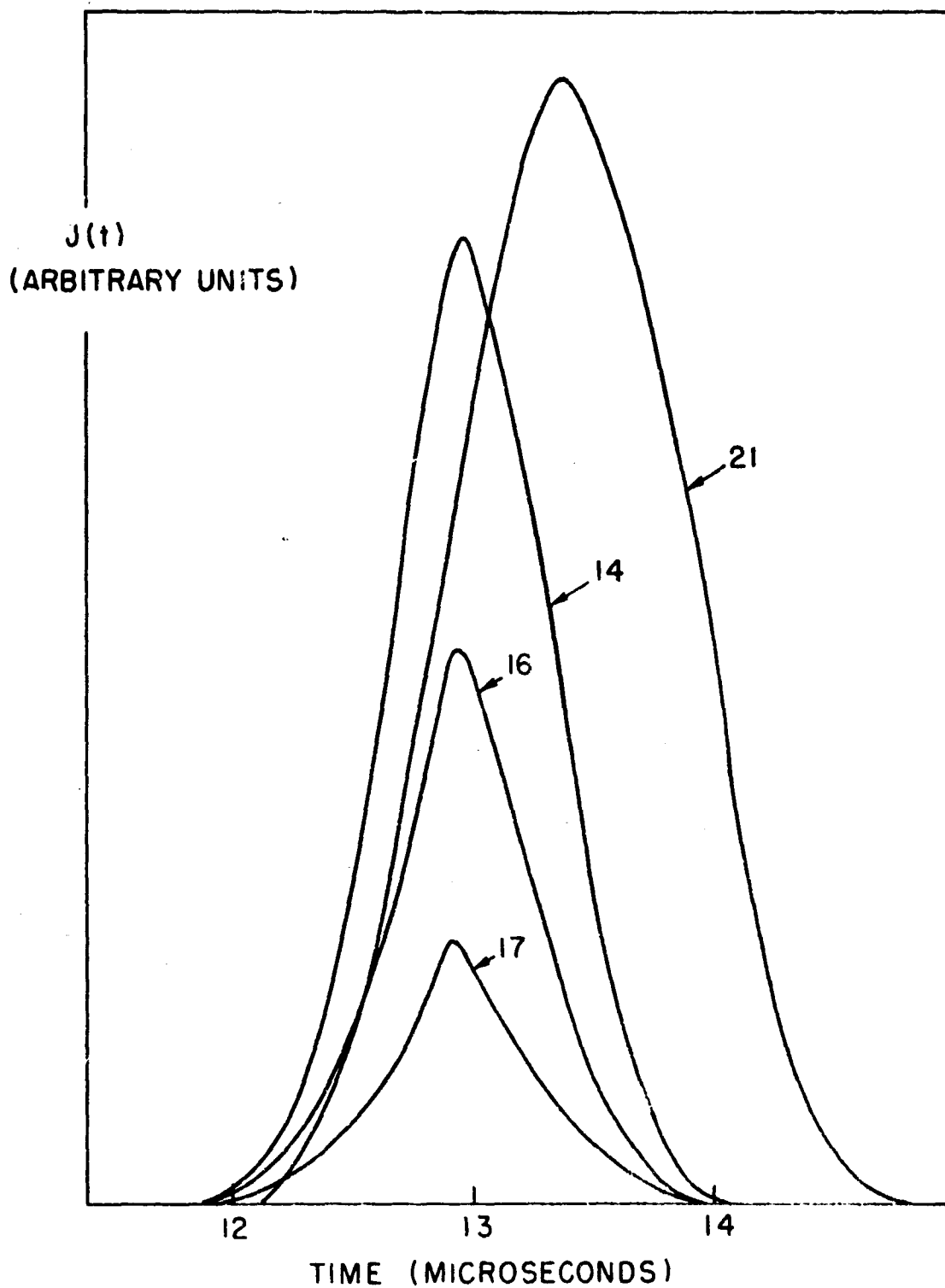
Figure III-7 - Detector Pulse Shapes Claculated Using a Constant Emission F(t) and Constant Temperature. The Different Curves Represent Different Widths of F(t), from 50 to 1000 Nanoseconds. The Number on Each Identifies the Set of Parameters in Table III-2 Corresponding to that Curve.
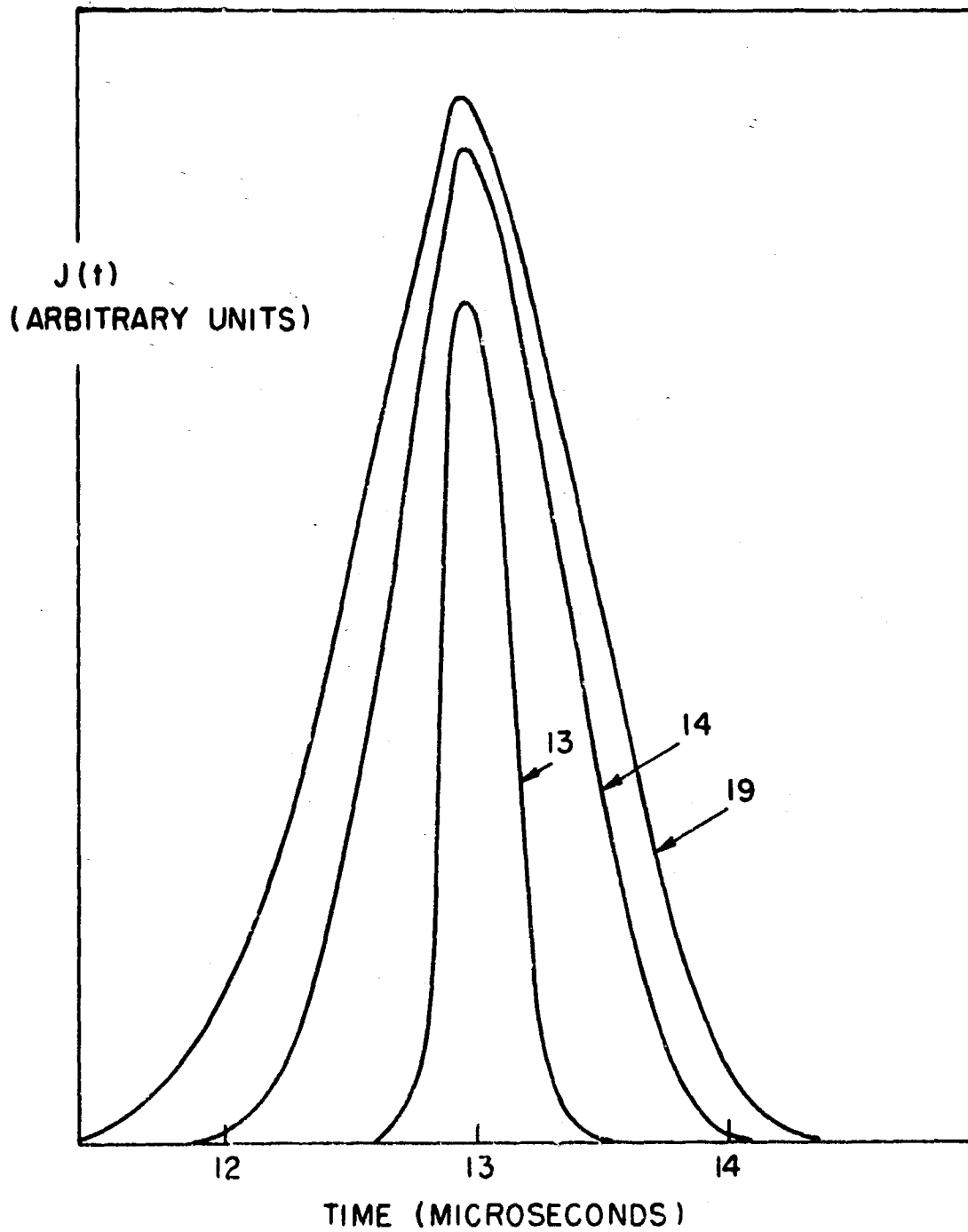
Figure III-8 - Detector Pulse Shapes Calculated Using a Constant Emission F(t) and Constant Temperature. Different Values of Temperature, from 10^4 to 2×10^5 °K. The Number on Each Identifies a Set of Parameters in Table III-2 Corresponding to that Curve.
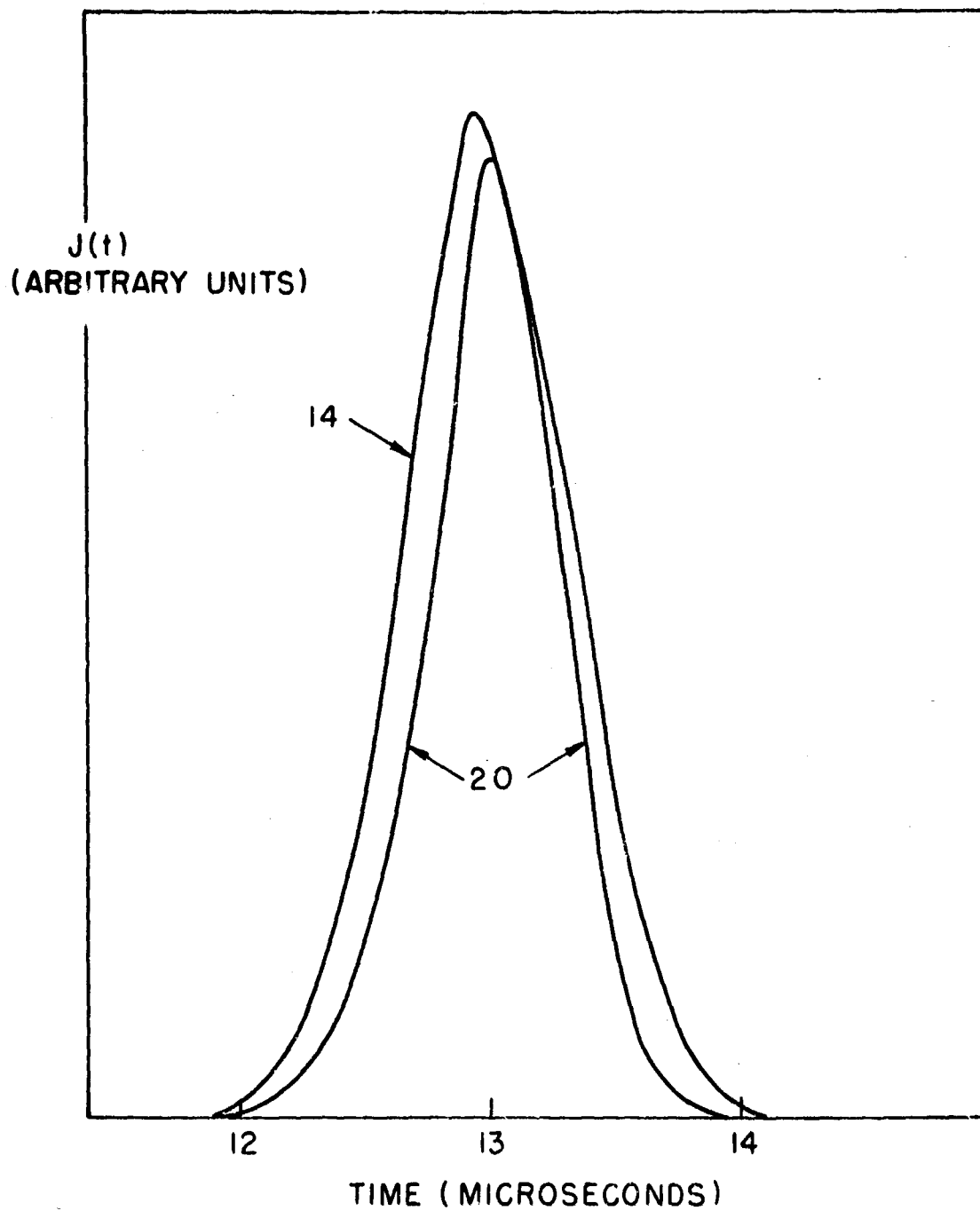
Figure III-9 - Detector Pulse Shape Calculated Using a Constant Emission F(t) and Time-dependent Temperature T(t). The Two Curves Represent Different Shapes for T(t). The Number on each Identifies a Set of Parameters in Table III-2 Corresponding to that Curve.
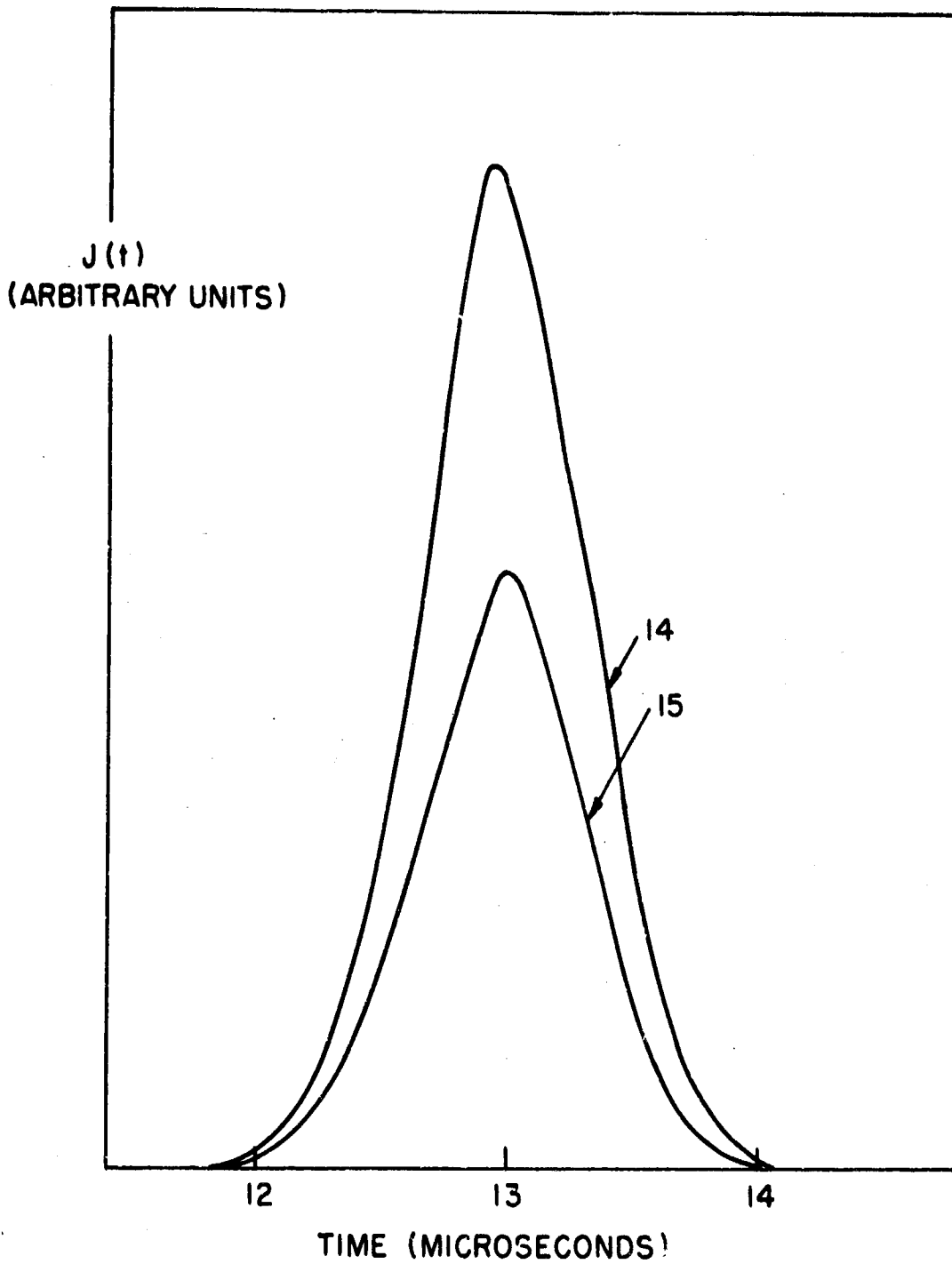
Figure III-10 - Detector Pulse Shape Calculated Using a Time-Varying Emission F(t) and Constant Temperature. The Two Curves Represent Different Shapes for F(t). The Number on Each Identifies a Set of Parameters in Table III-2 Corresponding to that Curve.

Section III A 2 using a δ function approximation were Maxwellian, we would expect, in these calculations, that as we shorten the length of the emission F(t), we should approach a pulse shape similar to that observed in the experiments. But this is not the case. We shall return to this point later.

In Figure III-8 we see the effect of increasing the temperature T(t) characterizing the Maxwellian from 10^4 to 2×10^5 degrees Kelvin, for flat F(t). At the lower end of this range, we find pulses too short to agree with experiment, and at the upper end pulses too long, but again the pulse shape does not change significantly.

In Figure III-9, we see the effect of changing the shape of T(t), without changing the peak value; again there is no great effect on the shape of J(t). In Figure III-10, we see the effect of changing the shape of F(t) here a detailed comparison of the curves shows that a triangular F(t) gives a J(t) that rises slightly more slowly than that given by a flat F(t), but the effect is not great.

As an extension of the ideas discussed in connection with Figure III-7 and as a further confirmation of the conclusions reached above we have taken F(t) to be a delta function and carried out the integration. The results are shown in Figure III-11. Curve 1 was obtained using the velocity distribution derived in the first use of the analysis described in Appendix I, which was similar to a Maxwellian; as noted before this was obtained with too coarse a mesh. Curve 2 was obtained using a Maxwellian velocity distribution with a temperature of 70,000 degrees Kelvin, and curve 3 was obtained using an asymmetric velocity distribution with a peak near the high velocity end of the distribution, similar to the types found in Section III A 1. Curves 1 and 2 are similar to those obtained above. The results of curve 1, in particular, show that the earliest results, which cannot indicate a velocity distribution similar to a Maxwellian, are not exactly right, since running the analysis backwards

-51-
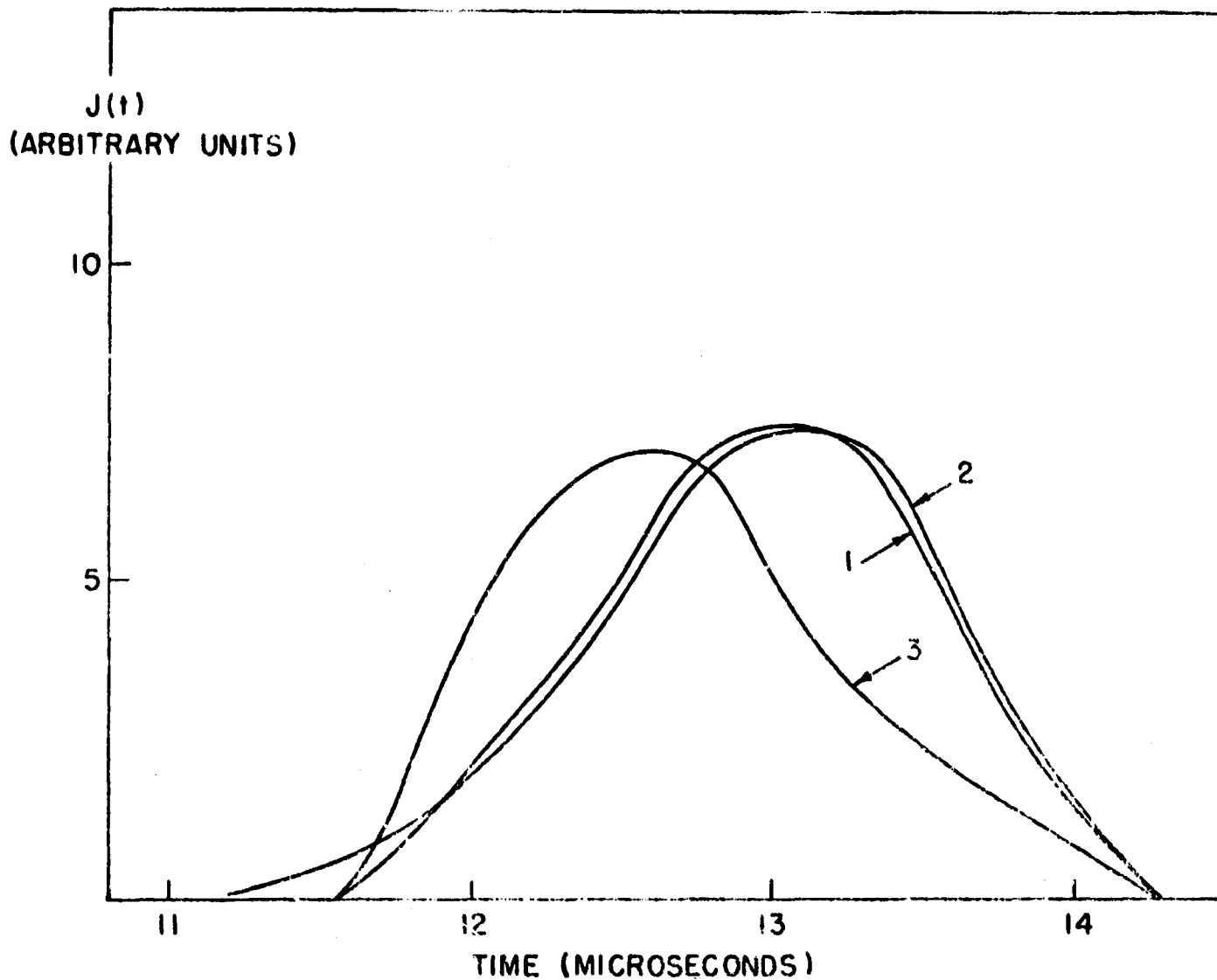
Figure III-11 - Detector Pulse Shapes Calculated Using a Delta Function for F(t) and Constant Temperature. Curve 1 is from a Quasi-Maxwellian, as described in text; curve 2 is from a Maxwellian at 70,000°K; curve 3 is from an asymetric velocity distribution peaked near the hig velocity end.

with the distribution obtained does not yield the original pulse shape $J(t)$. Curve 2 indicates that shortening the length of the emission $F(t)$ toward zero does not modify the pulse shape, as we said before in connection with Figure III-7. Curve 3 indicates that the experimentally observed pulse shape may be obtained with velocity distributions of the type found in Section III A 1 -- slightly asymmetric with peaks near the high velocity end.

Thus, this analysis so far indicates that the calculated pulse shape is not particularly sensitive to variation of the available parameters, so long as a Maxwellian velocity distribution is assumed. An exception to this statement may occur when $F(t)$ varies over a long emission time and $T(t)$ is low. Further work is in progress on this point. The preliminary results support the results of Section III A 1 where we found distributions that depart from Maxwellian form.

B. EXTENSION OF CALCULATIONS ON EFFECT OF INVERSE BREMSSTRAHLUNG

In the last semiannual report[1] we described calculations on the possible effect of heating of the blow-off material by free-free transitions of the electrons in the path of the laser radiation, and came to the conclusion that electron densities were too low to explain the high (200 ev) ion energies observed. In view of the results described above, in which it appears that the major portion of this energy is a directed energy, it appears worthwhile to re-examine this result to see if the random component, an order of magnitude lower, could possibly be explained by this mechanism. This would not serve to explain the directed component, but a random component of the order of 10-20 ev does appear to be similar to a thermal energy. This random energy also appears to be compatible with the temperatures deduced for the blow-off material using methods of optical spectroscopy.[6]

We consider two possible means by which the effects considered in the semi-annual report could be enhanced; i.e., increased absorption of light because of sodium and potassium ions emitted by the surface, and the possibility of inverse Bremsstrahlung with the electron scattering in an interaction with a neutral particle rather than an ion. The first involves the presence of alkali metal ions in the blow-off material; these materials which would be present as ions and not as neutral atoms would increase the ion density over the thermal ion density of the dominantly un-ionized blow-off material, and thus increase the absorption cross section for the light in the critical early stages where the heating is just beginning, and generally is not proceeding rapidly because of low charged particle densities.

This consideration involves a feedback from the empirical results into the theory. We would be using our knowledge of what the blow-off material actually consists of. The theoretical model then deals with a case more like what is actually realized.

Accordingly the computational model described in the semi annual report has been modified by adding to the ion density a term corresponding to an ion density of alkali metal ions. This added ion density is not increased as the temperature increases because we consider these materials to be essentially fully ionized when they are emitted from the surface. We estimate, from the experimental results, an alkali metal ion density of about $10^{12}/cm^3$ in the early stages of the development of the particle emission.

The results of these calculations appear in Figures III-12, 13 and 14. Figure III-12 is identical with Figure IV-5 of the semi-annual report[1] and represents the case without the added alkali ions for a low initial neutral particle density. Figure III-13 shows the effect of adding the additional ions; the temperature increases much more rapidly for a constant initial electron density, and the critical electron density for runaway heating

-54-
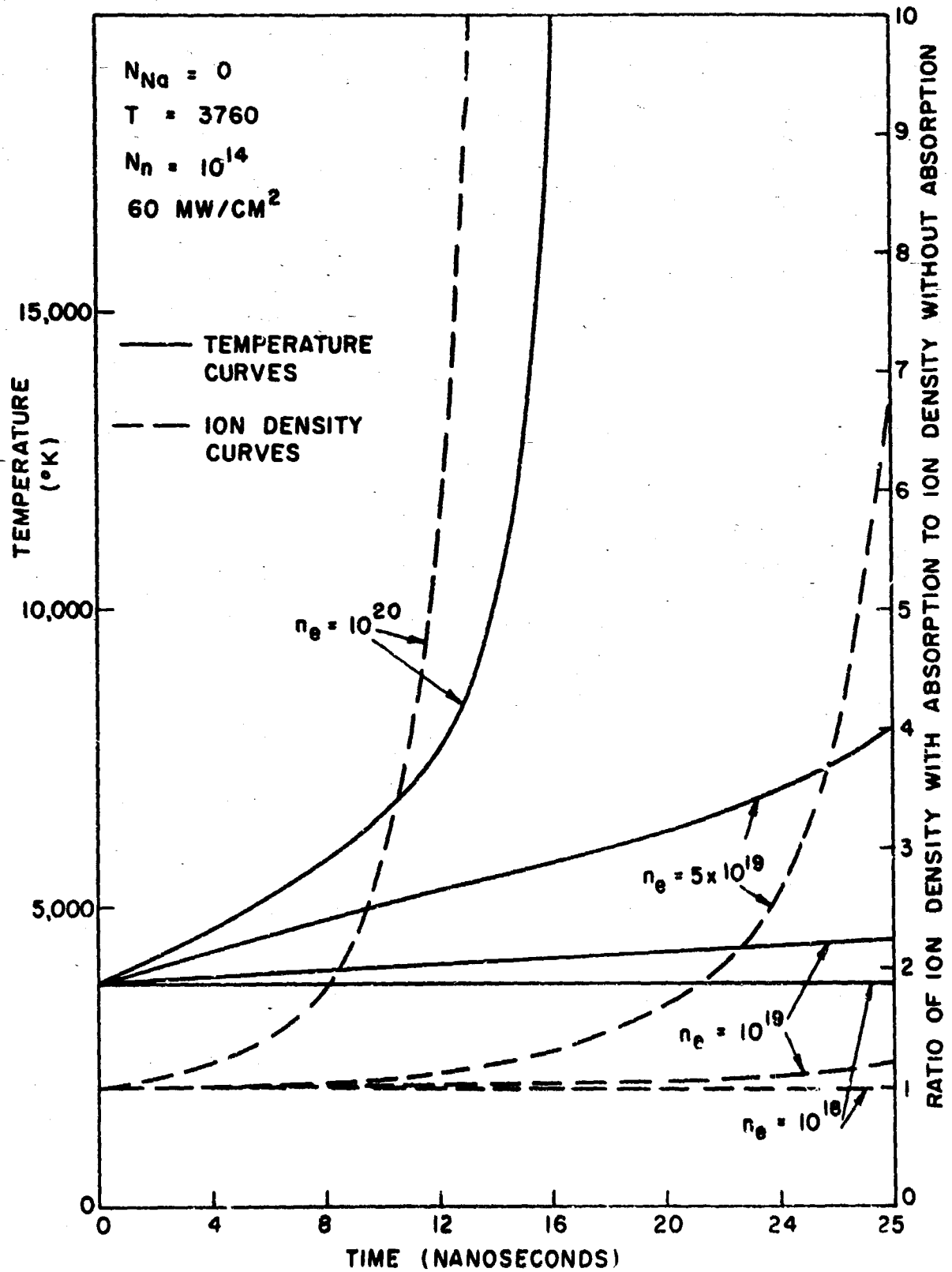
Figure III-12 - Calculated Plasma Heating by Inverse Bremsstrahlung.
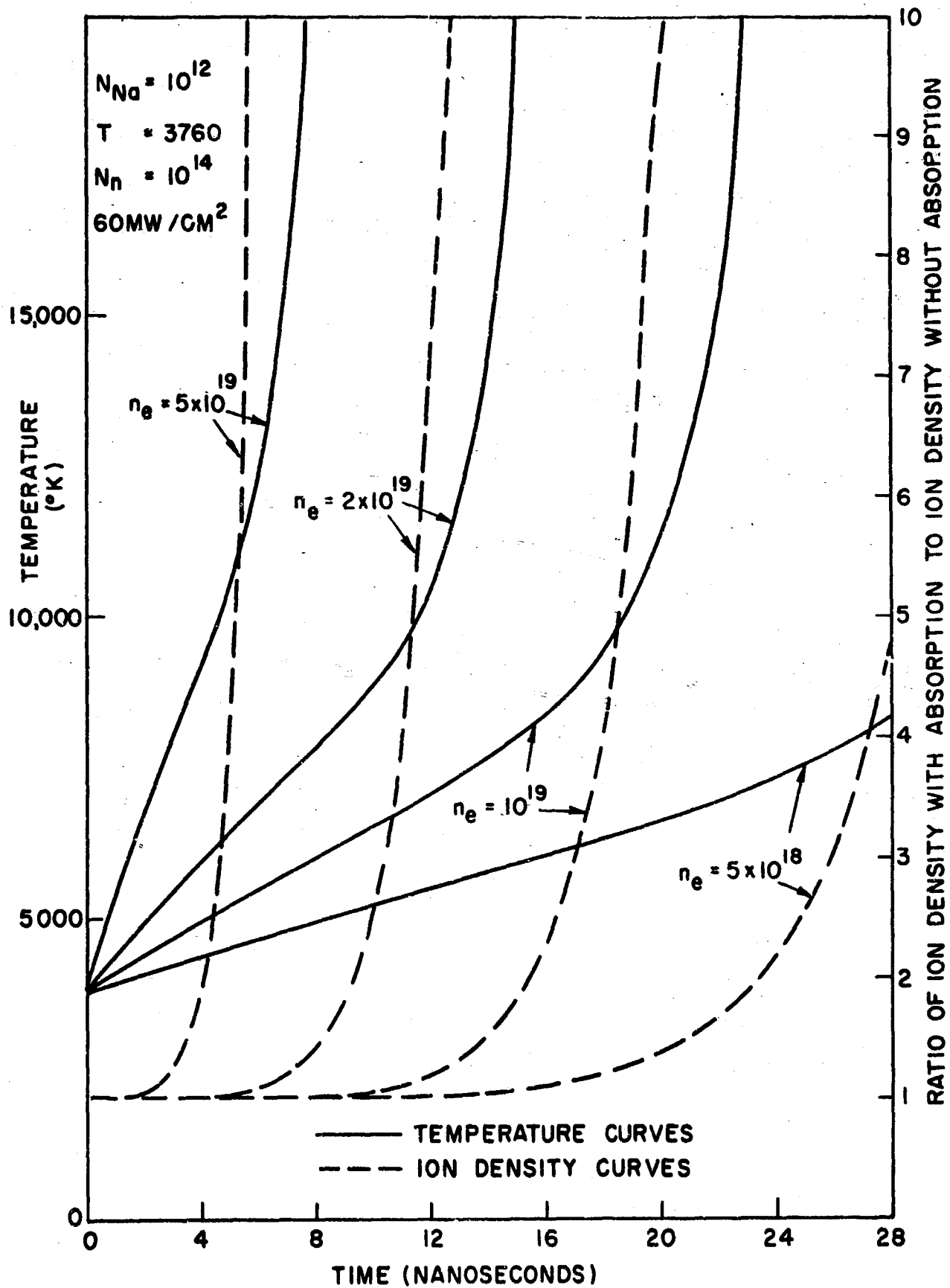
Figure III-13 - Calculated Plasma Heating by Inverse Bremsstrahlung in the Presence of Fully Ionized Sodium
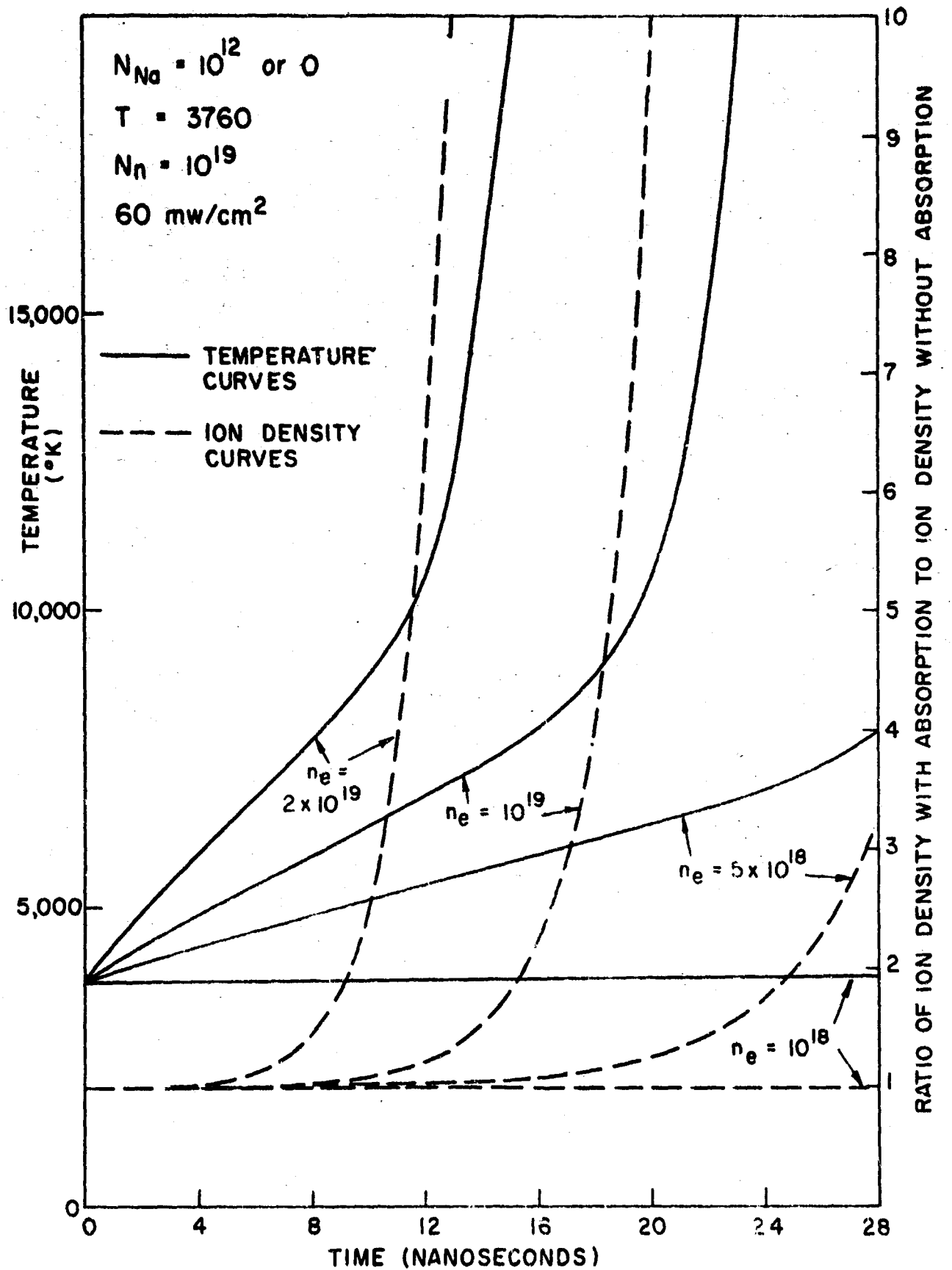
Figure III-14 - Effect of Increased Neutral Particle Density on Plasma Heating by Inverse Bremsstrahlung

during the period of the laser pulse is reduced by a factor of five. Figure III-14 shows the results at a higher initial neutral particle density. The curves are essentially the same for 10^{12} alkali ions/cm^3 as for 0. In this case, the addition of the alkali ions makes no difference since the thermal ionization yields an ion density greater than that of the ions. Comparison of Figures III-12 and III-13 shows that the critical electron density is reduced at higher initial neutral particle densities although the variation is rather slow. The conclusion is that the presence of the alkali metal ions should indeed make the heating proceed more rapidly, especially for relatively low particle densities, and that the restrictions on electron density for heating are eased somewhat. These changes by themselves, however, are not sufficient to reverse the conclusions in the semi-annual report.

Now let us consider the possibility of inverse Bremsstrahlung proceeding by interaction of the electron with a neutral particle rather than with an ion. There have been some recent results on the cross section for this process.[7] The cross section is smaller than for the process involving an ion, but this may be compensated by the much larger density of neutral particles which is available in the early stages of the process. When we also consider that we may be trying to explain a thermal energy of only 20ev rather than 200 ev as we were before, this additional process may be helpful. The analysis is now in the process of being carried out, but no results are available as yet.

The absorption coefficient k_ν for light in the slightly ionized blow-off material by the process in which the electron makes a free-free transition in the field of an ion was given in the semi-annual report;

$$k_\nu \text{ (ion)} = \frac{8\pi e^6 \left(\ln \Lambda \right) n_e n_i}{3c\nu^2 (2\pi mkT)^{3/2}} = 9.32 \times 10^{-31} \frac{n_i n_e}{T^{3/2}}$$

for the ruby laser frequency. Here n_e and n_i are electron and ion densities, T is the temperature of the material, ν is the frequency of the light, and $\ell n \, \Lambda$ accounts for collective effects and is approximately equal to 10. The symbols m, e, c, and k have their conventional meanings of electron mass, electron charge, velocity of light, and Boltzmann's constant.

For the free-free transition of an electron near a neutral hydrogen atom, the absorption coefficient has recently been evaluated[7] as

$$k_\nu \text{ (neutral)} = \frac{4.8 \, \hbar^{7/2}}{m^3 \, c \nu^{3/2}} \left(\frac{\pi}{3kT} \right)^{1/2} n_n \, n_e = 7.79 \times 10^{-38} \, n_n \, n_e / T^{1/2}$$

for the ruby laser frequency.

Here n_n is the density of neutral hydrogen atoms, and $\hbar$ is Planck's constant divided by 2π. This result is strictly valid only for atomic hydrogen; corresponding results for other gases are not available. One estimate[8] for molecular hydrogen indicates an absorption coefficient smaller by a factor of between two and four. An estimate for argon[9] indicates a factor smaller by a factor of four. However, if we assume that the absorption cross section for the other materials emitted as neutral gases (such as CO and CO_2 which are known to be produced copiously under our experimental conditions) is comparable to that of hydrogen, we are led to a large value of the absorption coefficient by this process; indeed, to a larger value than that due to the absorption in the field of an ion. The ratio of the absorption coefficients due to the two processes would be:

$$\frac{k_\nu \text{ (neutral)}}{k_\nu \text{ (ion)}} \approx 10^{-7} \, \frac{n_n}{n_i} \quad T.$$

Typically, for emission of the usual gases from a surface at a few thousand degrees Kelvin, we would expect

$$n_i/n_n \approx 10^{-6} \text{ to } 10^{-5},$$

so that the ratio defined above could be much greater than one. Thus, absorption in collisions of electrons with neutral atoms and molecules could easily dominate over absorption in collisions with ions. If this were to occur, the critical electron density at which heating occurs rapidly could be lower than calculated in the semi-annual report.

The computations based on these considerations are similar to those based on the absorption in collisions with ions described in the semi-annual report. The experimental studies of neutral gas desorption allow realistic estimates of neutral particle density as a function of time near the surface. The result of carrying out this procedure with the larger absorption coefficients may predict sufficient heating to explain the random component of the velocity distributions described earlier, but they are unlikely to explain the directed component.

C. TENTATIVE IDENTIFICATION OF HIGH SPEED NEUTRAL MOLECULES EMITTED FROM TUNGSTEN

Let us now consider the nature of the particles contained in the neutral pulses. We use the results obtained in Section III A 2 on the data of Figure III-4. In that section we obtained results for the energy in terms of the mass number A for both the directed and random components.

If we were to assume that the first neutral particle pulse was CO, an assumption that might seem plausible since CO is the most abundant component observed in the gas phase emitted from tungsten, we note that the

directed energy would be approximately 1270 ev. This does not seem reasonable since the energy would be much higher than that found in the measurements on ions in the time of flight instrument. Moreover, let us consider the ratio of the masses represented by the two pulses. If we assume that the two peaks represent approximately the same energy, we find

$$\frac{1}{2} \; m_1 \left(\frac{d}{t_1}\right)^2 \; = \; \frac{1}{2} \; m_2 \left(\frac{d}{t_2}\right)^2 \, ,$$

where t_i is the time of arrival of mass m_i (measured at the peak of the pulse) and d is the distance from target to detector. Then

$$\frac{m_2}{m_1} \; = \; \left(\frac{t_2}{t_1}\right)^2 \, .$$

At the peaks of the pulse $t_1 = 6.04 \mu s$, $t_2 = 22.2 \mu s$, leading to $m_2/m_1 = 13.5$. If the first pulse were CO, the second would then have a mass number of almost 380, an unreasonably high value. If we were to assume the second pulse to be CO, the first would then be mass 2 which would correspond to H_2. This appears to be a reasonable component to be emitted. If the identities of these two pulses are H_2 and CO, the energies are, according to the results of Section III A 2, 78 and 44 ev for the directed components, and 5.4 and 12.6 ev for the random components.

These energies are not in perfect agreement, they violate the assumption of equal energy for the two pulses which we advanced above. They are also somewhat lower than the energies found in the ion emission work, but the 78 ev for H_2, at any rate, differs only by a factor of 2 from the ion energies. These energies, at any rate, appear to be more plausible than the 1270 ev found by postulating that the first pulse is CO. There are no other reasonable mass assignments for these two peaks differing by a factor of 14. In addition, as we noted in Section I, there is evidence for identifying the first neutral molecule peak from titanium as hydrogen. Clearly a considerable amount of additional work is required to explain these results.

SUMMARY

The work described in this report deals with the measurement of particle emission from metal surfaces irradiated with light flux densities of 50-70 Mw/cm^2, as well as calculations of the velocity distribution of the particles from the measured pulse shapes. Measurements in the quadrupole mass spectrometer have shown that, besides the thermal gas desorption, the neutral particle emission contains a photon pulse and several high velocity non-zero-mass pulses. Tentative assignments of masses and energies of the high speed neutral pulses are made.

The electric field dependence of the time of flight of ions emitted from tungsten and platinum surfaces were measured, and it was concluded that they behave as independent particles in their response to electric fields. The ion mass spectra obtained from platinum were very similar to those from tungsten with respect to both mass and energies observed. Other measurements on platinum suggest that an interaction of the blow-off particles with the laser beam is required for the production and acceleration of ions.

Analysis of the measured pulse shapes for both ions and neutrals yields velocity distributions with random energies of a few tens of electron volts superimposed on a directed energy of hundreds of electron volts. Calculations of heating of the blow-off material by inverse Bremsstrahlung have been extended to the case of a multi-component system, with one of the components being a fully ionized alkali metal.

REFERENCES

1. "Mechanisms of Laser Surface Interactions", by J. F. Ready, E. Bernal G., and L. P. Levine, Semi-Annual Report to Ballistic Research Laboratories on Contract No. DA-11-022-AMC-1749(A), Modification No. 2, November, 1965.

2. A. Rostagni, Il Nuovo Cimento, 11, 99 (1934)

3. S. C. Brown, Basic Data of Plasma Physics, John Wiley and Sons, New York (1949)

4. Final Report, "Mechanism of Laser-Surface Interactions" by J. F. Ready, E. Bernal G., and L. P. Levine, to Ballistic Research Laboratories on Contract No. DA-11-022-AMC-1749(A), March, 1965.

5. R. V. Churchill, Operational Mathematics, McGraw-Hill, New York, N. Y. (1958)

6. E. Archbold and T. P. Hughes, Nature, 204, 670 (1964)

7. P. R. Browne, Proc. Phys. Soc., London, 86, 1323 (1965)

8. W. B. Somerville, Astrophys. Jour. 139, 192 (1964)

9. A. V. Phelps, R. W. Waynant, J. H. Ramsey, "Technical Report #RADC-TR-65-133", June 1965 (AD-467392)

APPENDIX I

ION VELOCITY DISTRIBUTION FROM MEASURED MASS PULSES

The material in this appendix consists of unpublished work by Frank J. Allen of Ballistic Research Laboratories. It is included here because we draw heavily on its contents, and the material is not available elsewhere. We have edited and condensed the original, retaining only those parts required for use in this report.

Suppose the particles vaporized by the laser pulse, whether neutral or ionized initially, form a dense plasma close to the target surface. Many interactions take place here; the particles also undergo collisions with the target surface. The result of all this is assumed to be: ions, electrons, and neutral atoms (and in some cases more complex species) attain random velocities superposed upon a directed component of velocity normal to the surface. We might expect for each species a Maxwellian distribution about the directed component, but this must be decided by the experimental results.

The ions after leaving the plasma, i.e, after getting far enough from the target surface so that the density is low and collisions in which significant momentum is transferred are infrequent, are accelerated in an electric field and ultimately those traveling in a very small solid angle about the normal to the target surface are detected. Under these conditions we might expect that the more energy the ions have, the higher will be both their random velocities and the superposed directed velocity normal to the target surface.

Before considering a distribution of ion velocities, consider the detection of a single pulse of ions with velocity W normal to the target surface. The ions travel one dimensionally in a region consisting of an arrangement of grids with potentials which are completely arbitrary except for the restriction that the ions not be reversed in direction, i.e., the ions are allowed to reach the detector at the end of the region. Let ρ, v, J be the ion density, velocity, and current and V the field potential. Then the governing equations are:

$$\frac{\partial J}{\partial x} = -\frac{\partial \rho}{\partial t} \tag{1}$$

$$J = \rho v \tag{2}$$

$$\frac{1}{2} m \left[v^2(x) - W^2 \right] = e \left[V(x) - V(0) \right] \tag{3}$$

where e is the ion charge.

The "initial current" is $J(0,t) = \rho(0,t) \, w$. Now the ions emitted at time t
(i.e., leave the plasma without further collisions) reach a point x at a time
$t + \tau$ where

$$\tau(x) = \int_0^x \frac{dx}{v(x)} \qquad (4)$$

where $v(x) = \sqrt{\frac{2e}{m} \left[V(x) - V(0) \right] + w^2} \qquad (5)$

Now the ions emitted in time dt at $x = 0$ fill a tube of length $w\,dt$ while at
time $\tau(x)$ later these same ions fill a space $v(x)\,dt$. But the number
crossing a plane at (x, t) must be the same as the number emitted at $(0, t-\tau)$. So

$$J(x,t) = \rho(x,t) \, v(x) = \rho(o, t-\tau) \, w = J(o, t-\tau) \qquad (6)$$

It is readily verified that this prescription satisfies the continuity equation:

$$\frac{\partial J}{\partial x} = w \, \frac{\partial \rho(o, t-\tau)}{\partial(t-\tau)} \times \frac{\partial(t-\tau)}{\partial x}$$

$$= w \, \frac{\partial \rho(o, t-\tau)}{\partial(t-\tau)} \cdot \frac{-\partial\tau}{\partial x}$$

But $\tau(x) = \int_0^x \frac{dx}{v(x)}$

So $\frac{\partial\tau}{\partial x} = \frac{1}{v(x)}$

Thus $\frac{\partial J}{\partial x} = - \left| \frac{w}{v(x)} \times \frac{\partial\rho(0, t-\tau)}{\partial(t-\tau)} \right.$

-65-

Now from equation (5):

$$-\frac{\partial \rho}{\partial t} = \left(\frac{-w}{v(x)}\right) \frac{\partial \rho(0, t-\tau)}{\partial(t-\tau)} \times \frac{\partial(t-\tau)}{\partial t}$$

$$= \left(\frac{-w}{v(x)}\right) \frac{\partial \rho(0, t-\tau)}{\partial(t-\tau)}$$

So $$\frac{\partial J}{\partial x} = -\frac{\partial \rho}{\partial t}$$

Thus the governing equations are satisfied no matter how many grids there are, where they are, or what the potentials are, provided only the potentials are such as to allow the ions to reach the detector. This condition implies $v(x) > 0$ and $\tau(x) > 0$.

To recapitulate, the solution is

$$J(x, t) = \rho(x, t) \, v(x) = \rho(0, t-\tau) \, w = J(0, t-\tau)$$

$$\tau(x) = \int_0^x \frac{dx}{v(x)}$$

$$v(x) = \sqrt{\frac{2e}{m} \left[V(x) - V(0)\right] + w^2} \qquad (7)$$

Since it is assumed that:

$$\rho(0, t) = 0 \text{ for } t < 0,$$

$$J(x, 0) = 0.$$

This solution has the important property that the current pulse $J(x, t)$ suffers no distortion at any point in the flow field; the (retardation) time $\tau(x)$ depends upon the grid and potential arrangement, but the current pulse $J(x, t) = J(0, t-\tau)$.

Consider now a case in which the ions leave the plasma with some distribution of speeds in the x direction with the same other conditions as previously. (The ions with significant y and z components will not be detected).

Let w = speed in x direction ion has upon escaping from plasma.

Let $\rho (0, w, t)$ = density per unit initial speed.

$J(0, w, t)$ = current per unit initial speed.

Let $\rho (x, v, t)$ = density per unit ion speed v.

$J (x, v, t)$ = current per unit ion speed v.

Then
$$J(0, t) = \int_{w=0}^{\infty} \rho (0, w, t) \, w \, d w = \int_{0}^{\infty} J(0, w, t) \, dw \qquad (8)$$

$$J (x, t) = \int_{0}^{\infty} \rho (x, v, t) \, v (x) \, dv = \int_{0}^{\infty} J (x, v, t) \, dv \qquad (9)$$

By analogy with the solution for the constant velocity case it then appears that the solution for this case should be given by the following prescription:

$$J(x, t) = \int_{0}^{\infty} \rho \left[0, w, t, - \tau (x, w) \right] w \, d w$$

$$\tau (x, w) = \int_{0}^{x} \frac{dx}{v (x, w)} \qquad (10)$$

$$v (x, w) = \sqrt{\frac{2e}{m} \left[V(x) - V(0) \right] + w^2}$$

Again $\rho (0, w, t) = 0$ for $t < 0$,

and $v (x, w) > 0$, $\tau (x, w) > 0$.

for all detected ions. Then $J (x, 0) = 0$ as before.

Again it may be shown that this physically obtained solution satisfies the continuity equation by differentiating J (x, t) as required. It is helpful to note that vdv = wdw in carrying out the procedure. The procedure is the same as previously and will not be repeated.

A. DELTA FUNCTION APPROXIMATION FOR EMISSION PULSE

The solution given is mathematically correct for any arbitrarily prescribed function J (0, w, t). However, the physical problem is to find J (0, w, t) from the experimentally determined J(x, t). This cannot be done uniquely; some assumption has to be made about J(0, w, t). Since the laser pulse is short and the laser-induced plasma has a fleeting existence, the most obvious assumption is that J(0, w, t) is a delta function in time. This appears reasonable when the time spread in the mass peak is long compared with the laser pulse time. (The lighter mass peaks could be spread out somewhat in time by lowering the accelerating potential; this procedure is limited by the rather high constant speed of the plasma normal to the target surface on which the random motions are superimposed, and by the decrease of solid angle in which emitted ions are detected).

For cases in which a delta function in time cannot be assumed, one no longer has a one-to-one correspondence between escape velocity w and time of detection t. This correspondence leads to a considerable simplification in the nature of the solution given by Eq. (10). We consider the case first therefore in which the ions escape the plasma as a δ function in time.

For this case it is simpler, and physically more satisfying, to proceed directly rather than to use the solution for the more general case. First note that almost all of the time the ions spend in getting from the plasma to the detector is spent in the drift tube where each ion has a constant velocity. This constant velocity is determined by

$$\frac{1}{2} m w^2 + e \left[V (x_d) - V (0) \right] = \frac{1}{2} m v^2 \tag{11}$$

where v is the velocity in the drift tube and $V(x_d)$ = potential throughout drift tube. w is the ion velocity upon escaping the plasma and is distributed in some way about some mean plasma speed away from the target surface. Since the detector position is fixed, we replace J (x, t) by J(t), the detected current.

Let N(w) = the number of ions escaping plasma per unit escape velocity per square centimeter during the delta function escape time.

$$\text{Let } N = \int_0^\infty N(w) \, dw \tag{12}$$

In the previous notation (13)

$$N = \int J\,(0, w, t)\,dw\,\delta(t)\,dt = \int J\,(0, w, 0)\,dw$$

Then $\quad N(w)\,\left|dw\right| = J(t)\,\left|dt\right|$ (14)

where t and w are related since t is the time spent in the drift tube by an ion of initial escape speed w. In this section we make the approximation that the time not spent in the drift tube doesn't contribute to the spreading of the mass peak; if the time of detection is measured with respect to the laser pulse zero time, the time not spent in the drift tube is a constant to be subtracted from the total time in using the relationship between t and w.

We thus have

$$t = \frac{\text{length of drift tube}}{\text{velocity in drift tube}} = \frac{x_d}{v}$$ (15)

or $\quad t = \dfrac{x_d}{\sqrt{\dfrac{2e}{m}\left[V(x_d) - V(0)\right] + w^2}}$ (16)

and $\quad \dfrac{dt}{dw} = -\dfrac{x_d w}{v^3} = -\dfrac{x_d w}{\left(\dfrac{x_d}{t}\right)^3} = -\dfrac{t^3}{x_d^2}\,w$ (17)

Then $\quad \dfrac{N(w)}{w} = J(t)\,\dfrac{t^3}{x_d^2}$ (18)

with $\quad w = \sqrt{\left(\dfrac{x_d}{t}\right)^2 - \dfrac{2e}{m}\left[V(x_d) - V(0)\right]}$ (19)

Equations (18) and (19) give the distribution function $N(w)$ in terms of the measured current, apart from a multiplicative constant which depends on system parameters, for example, transparency losses at grids, detector sensitivity, etc.

We also wish to find expressions for the average velocity and average energy. In getting the energy we must remember that we are detecting only ions whose y and z components of velocity are essentially zero. We assume however, that the x components are independent of the y and z components as regards the random part of the distribution, the latter being superimposed on a drift velocity having only an x component. Then the average ion energy measured may be manipulated as follows:

$$\overline{E} = \frac{1}{2} m \frac{\sum w^2 N(w) dw}{\sum N(w) dw}$$

$$\overline{E} = \frac{1}{2} m \frac{\sum [\overline{w} + (w-\overline{w})]^2 N(w) dw}{N}$$

$$= \frac{1}{2} \frac{m}{N} \sum [\overline{w}^2 + 2\overline{w}(w-\overline{w}) + (w-\overline{w})^2] N(w) dw$$

$$= \frac{1}{2} m \overline{w}^2 + \frac{1}{2} \frac{m}{N} \sum (w - \overline{w})^2 N(w) dw$$

where $N = \sum N(w) dw$

and $\overline{w} = \dfrac{\sum w N(w) dw}{N}$ (19a)

Thus $\overline{E}$ is decomposed into a center of mass energy and the mean energy (x component) about the center of mass motion. According to the assumption made, the y and z components of motion would give rise to energies equal to the random part of the x distribution. Then the mean total energy of the ions including all components would be

$$\overline{E}_{total} = \frac{1}{2} m \overline{w}^2 + \frac{3}{2} \frac{m}{N} \sum (w - \overline{w})^2 N(w) dw$$ (19b)

B. FINITE WIDTH FOR EMISSION PULSE

In the more general case, where there is not a one-to-one correspondence between escape velocity w and time of detection t, the solution (10) cannot determine the distribution of ions escaping over both velocity and time solely by use of the detected current. Additional assumptions concerning the ion distribution must be made. One could assume certain properties, for example, a Maxwellian distribution of initial escape velocities corresponding to some temperature which may or may not vary with time of escape or one could assume an escape rate which could be a square pulse, or have the laser pulse shape.

Free parameters such as the temperature of the distribution or a constant multiplicative factor of the number escape rate could then be adjusted in accordance with the detected current after the integration called for in Eq. (10) has been performed.

Perhaps the easiest way to see the complexity involved in using the solution (10) when the ions do not escape the plasma in an essentially zero time interval is to assume that they escape at two discrete times t'_1 and t'_2.

Let $f_1 (t'_1)$ = number of ions/cm^2 which escape at t'_1,

$f_2 (t'_2)$ = number of ions/cm^2 which escape at t'_2,

$N_1 (w)$ = number/unit escape velocity for ions escaping at t'_1,

$N_2 (w)$ = number/unit escape velocity for ions escaping at t'_2,

Consider the currents measured at times t_1 and t_2. Let w_{11}, w_{21}, w_{12}, and w_{22} be the escape velocities for ions emitted at t'_1 and t'_2 and reaching the detector at t_1 and t_2. The second subscript refers to the times t_1 and t_2, and the first subscript to the times t'_1 and t'_2. Then,

$$J(t_1) \left| dt_1 \right| = f_1(t'_1) N_1 (w_{11}) \left| dw_{11} \right| + f_2 (t'_2) N_2 (w_{21}) \left| dw_{21} \right|$$

(20)

$$J(t_2) \left| dt_2 \right| = f_1 (t'_1) N_1 (w_{12}) \left| dw_{12} \right| + f_2 (t'_2) N_2 (w_{22}) \left| dw_{22} \right|$$

Now

$$t_1 - t'_1 = \frac{x_d}{\sqrt{\frac{2e}{m}\left[V(x_d) - V(0)\right] + w_{11}^2}} = \frac{x_d}{v_{11}} \tag{21}$$

$$\left|\frac{dt_1}{dw_{11}}\right| = \frac{x_d w_{11}}{v_{11}^3} = \frac{x_d w_{11}}{\left(\frac{x_d}{t_1 - t'_1}\right)^3} = \frac{w_{11}(t_1 - t'_1)^3}{x_d^2}$$

and

$$\left|\frac{dw_{11}}{dt_1}\right| = \frac{x_d^2}{w_{11}(t_1 - t'_1)^3} \tag{22}$$

Similar expressions hold for $\left|\dfrac{dw_{21}}{dt_1}\right|$, $\left|\dfrac{dw_{12}}{dt_2}\right|$, and $\left|\dfrac{dw_{22}}{dt_2}\right|$.

Now consider specific cases concerning what assumptions need be made to enable $J(t)$ to determine the remaining quantities.

(a) Suppose t'_1, t'_2, $N_1(w)$, $N_2(w)$, are known. Compute w_{11}, w_{21}, w_{12} and w_{22} along with $\left|\dfrac{dw_{11}}{dt_1}\right|$, etc. from (21) and (22). Then $J(t_1)$ and $J(t_2)$ determine $f_1(t'_1)$ and $f_2(t'_2)$. If there were i discrete ion pulses, i measured values $J(t_i)$ would determine $f_i(t'_i)$, provided the $N_i(w)$ were all known. More experimental values would over determine the $f_i(t'_i)$ and a least squares fit could be made.

(b) A different situation holds if we regard t'_1, t'_2, $f_1(t'_1)$ and $f_2(t'_2)$ as known. Then from (20) we cannot solve for $N_1(w_{11})$, $N_2(w_{21})$, $N_1(w_{12})$ and $N_2(w_{22})$. Two additional relations would be needed. For i ion pulses and i measured values $J(t_i)$, i (i - 1) additional relations would be needed.

On the other hand if we assume $N_1(w)$, say, is Maxwellian (or any given distribution) then this applies to $N_1(w_{11})$, $N_1(w_{12})$, $N_1(w_{1i})$ for all times t_i at which currents $J(t_i)$ detected are to be used. If we assume i distribution functions $N_i(w)$ corresponding to i times t'_i for which the $f_i(t'_i)$ are assumed known and then use i experimentally determined points $J(t_i)$ we would be able to determine the temperature T_i in each of the i distributions and hence in the limit find $T(t')$, i.e., the temperature of the assumed Maxwellian distribution as a function of time of escape from the plasma.

In general, one would not trust the information obtained when so much must be assumed. The difficulty is that one detects the current as a function of only one variable, time, whereas the ions escape the plasma in a distribution of two variables, velocity and time (and a third, space, which we have ignored because the ions all originate or escape the plasma very near to the target surface; a small potential correction could be applied here if it turns out that the distance from the target is at all significant).

However, while more must be assumed to exploit the general solution (10) than must be assumed for a delta function distribution in time, the delta function is a more drastic assumption, at least for the lighter ions where the time interval of the mass peak is not greatly longer than the laser pulse.

Therefore, the most reasonable procedure is to assume a delta function pulse in time as a first approximation. If higher accuracy seems achievable, one could then use the general solution (10) using a square pulse approximating the laser pulse, or a triangular pulse to approximate it, for the ion emission per unit time during the pulse then assume a Maxwellian velocity distribution with a temperature varying in time. There would appear to be no difficulty, in principle, in carrying out this procedure provided a number of discrete time intervals are used to approximate the ion emission. If an analytical choice of pulse shape is made, it would be better to integrate (10) at the outset and set the resulting function of time equal to $J(t)$.

However, while t is a parameter in the integral in equation (10) giving the detected current as a function of time, we find that taking the simplest case -- a square emission pulse in time --

$$J(0, w, t) = \rho(0, w, t) w$$

$$= A(t) f(w)$$

with $A(t) = A_0 \quad 0 < t < T$

$$0 \quad t < 0$$

$$t > T$$

and putting this into the solution (10), in general, one cannot perform the integration. Taking $f(w)$ to be a (one dimensional) Maxwellian

$$f(w) = \left[\frac{m}{2 \pi k\, T(t)} \right]^{1/2} w^2 \exp\left[- \frac{m\, w^2}{2\, k\, T(t)} \right] ,$$

a special although perhaps the most interesting case, does not help. We arrive at an expression

$$J(t) \quad \int_{w_{min}(t)}^{w_{max}(t)} A_0 \left[\frac{m}{2 \pi k\, T(t-\tau)} \right]^{1/2} w^2 \exp\left[- \frac{m\, w^2}{2\, k\, T\, (t-\tau)} \right] dw \quad (23)$$

T a function of $[\, t \quad \tau\,(w)\,]$

where $w_{min}(t) \quad \sqrt{ \left(\frac{x_d}{t} \right)^2 \quad \frac{2e}{m} \left[V\,(x_d) \quad V(0) \right] }$

$$w_{max}(t) \quad \sqrt{ \left(\frac{x_d}{t \quad \tau} \right)^2 \quad \frac{2e}{m} \left[V\,(x_d) \quad V(0) \right] }$$

Starting with equation (20) $J(t)$ may alternatively be expressed as an integral over time of escape from the plasma:

$$J(t) \quad \int_0^T A_0 \left[\frac{m}{2 \pi k\, T(t')} \right]^{1/2} w^2 \exp\left[- \frac{m\, w^2}{2\, k\, T(t')} \right] \quad \frac{x_d^2}{w(t - t')^3} x \quad dt'$$

where $\quad w^2 \quad \frac{x_d^2}{(t - t')^2} \quad \frac{2e}{m} \left[V(x_d) \quad V(0) \right]$

and $\quad \frac{dw}{dt'} \quad \frac{x_d^2}{w(t \quad t')^3}$

We see that if T is left as a function to be determined by J(t), but otherwise unspecified,

$$T = T[t - \tau(w)]$$

or

$$T = \tau(t')$$

the integrations cannot be carried out. If T is taken to be a constant, the integration can be performed. The time dependence of the integral is due to the fact that the limits of w are time dependent, not to any time dependence of the integrand. (In the alternative integral over t', w is a function of t so the integrand but not the limits are time-dependent). In either case the form of the function J(t) is specified by the integral and only the best fit of the detected current J(t) to the specified form can be obtained.

APPENDIX II

ION EMISSION FROM LASER IRRADIATED TUNGSTEN

(Paper presented at the F irth International Quantum Electronics Conference
Phoenix, Arizona, April ￼66)

In this paper we report on the emission of positive ions from tungsten surfaces irradiated with the output of a Q-switched laser in the range of 20-70 Mw/cm^2. The results on ion emission are only one part of a comprehensive study of the effect of laser irradiation on opaque surfaces at power levels for which the surface is not visibly damaged. Those parts of the study dealing with calculations of surface temperature upon irradiation, as well as electron emission from various metallic surfaces, have already been reported[1,2]. A report on the neutral particle emission is now being prepared.

Previous workers[3-6] have reported the observation of ions of the irradiated metal with energies up to a 1000 eV for light fluxes several orders of magnitude higher than those used in our experiments. At those power levels there is considerable evaporation of the metal and most of the emission consists of ions of the substrate material. We have measured the energy, masses and numbers of ions emitted from tungsten under conditions where most of the emission consists of species adsorbed on the surface. We find most of the ions to consist of Na^+ and K^+, some of which have energies up to 180 eV. Other ionic species are also found. The ratio of the ions to the total number of particles indicates that we are dealing with a lightly ionized gas.

Apparatus

A time-of-flight spectrometer with a decelerating grid in front of the detector has been used to measure the charge-to-mass ratio as well as the energy of the ions emitted by the surface during irradiation. The instrument is very well suited to this type of measurement because it can be used to display an entire mass spectrum for each laser pulse. Such a feature is highly desirable because of the difficulty in obtaining reproducible quantitative results from successive laser pulses. Figure 1 is a schematic of those parts of the spectrometer that are of interest here. A complete description of the construction details has been given elsewhere.[7] The metal to be studied, in sheet form, is used as an electrode and held 1.5 cm away from a one-meter long drift tube terminated in a disk shaped to approximate a Rogowski surface. On the opposite end of the drift tube is a decelerating grid, followed by a DuMont SPMO3-301 electron multiplier detector.
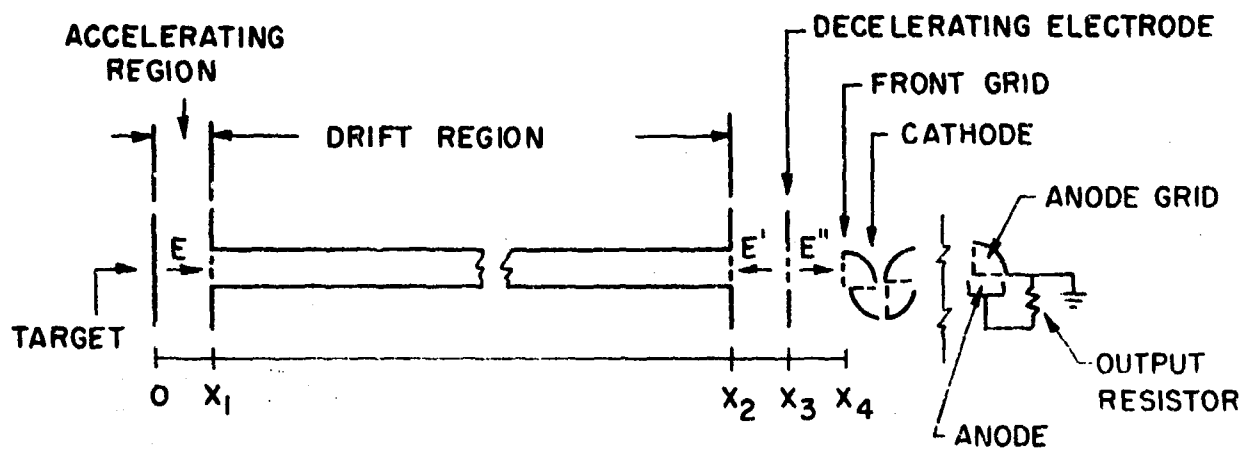
Figure 1 Appendix II - Schematic of Time of Flight Spectrometer
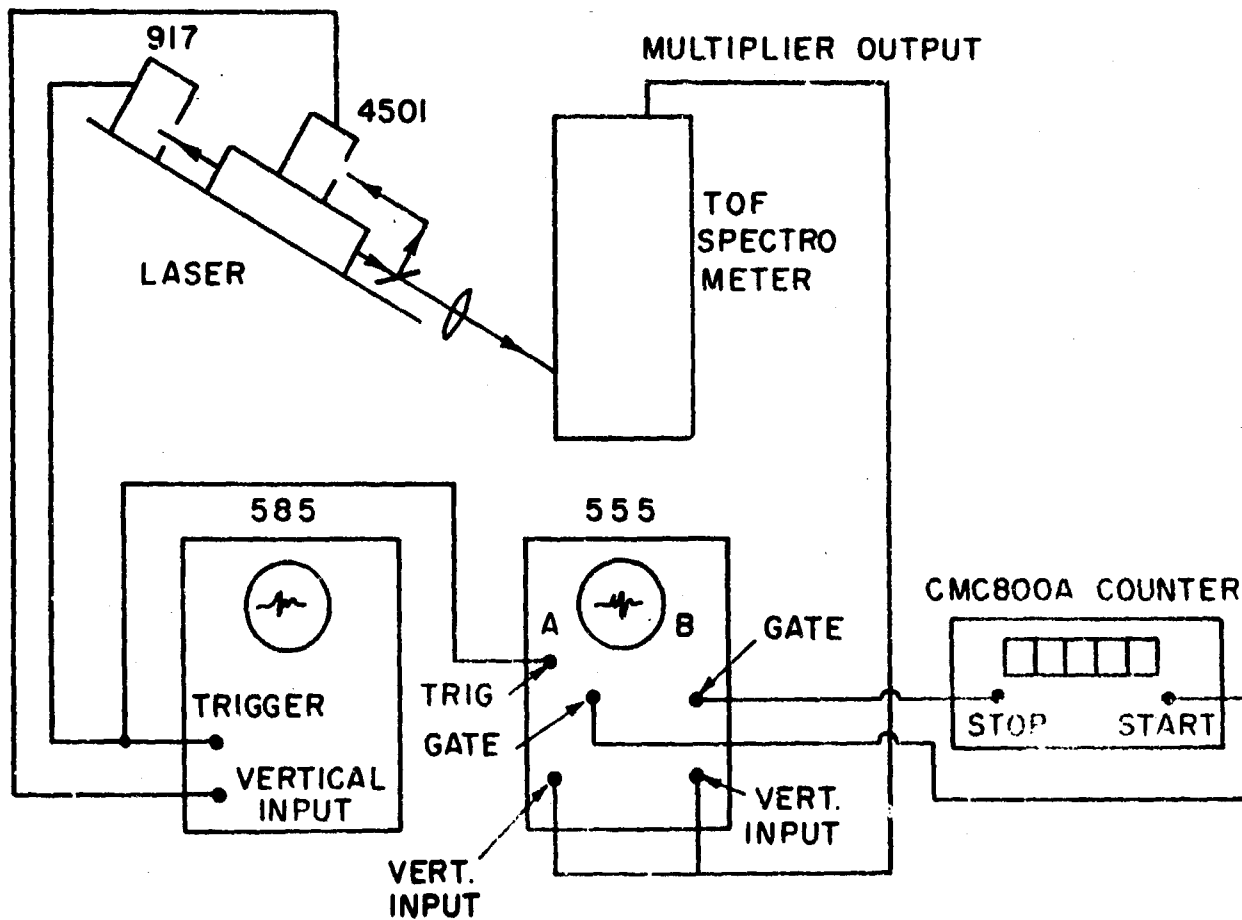
Figure 2 Appendix II - Experimental Arrangement for Measurement of Time of Flight
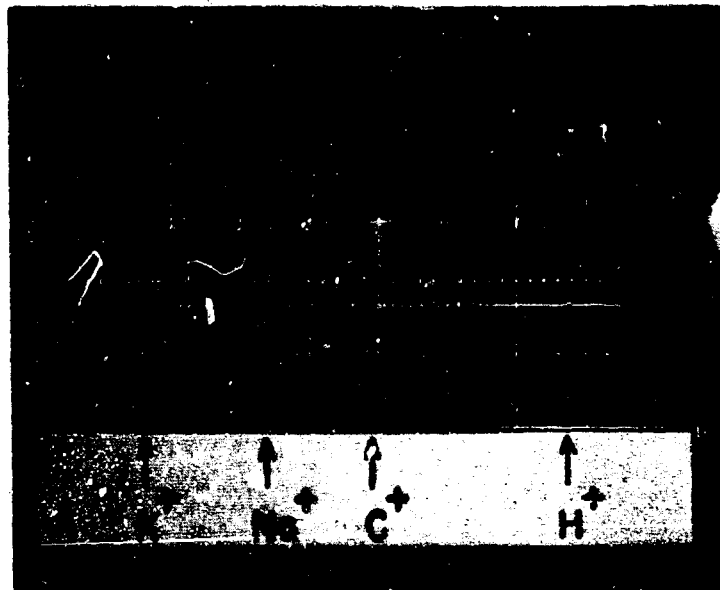
Figure 3a Appendix II - $E = E' = +1000V.$, vertical sensitivity of lower trace 0.2V/cm.
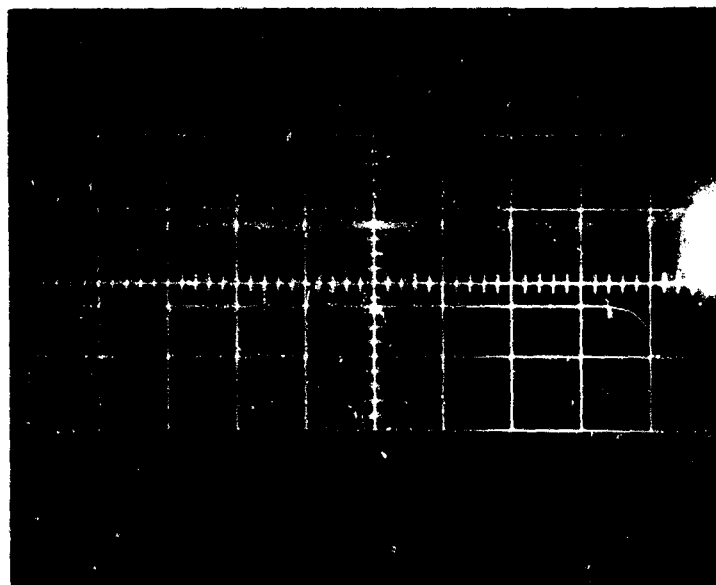
Figure 3b Appendix II - $E = =1000V.$, $E' = =1180V$, vertical sensitivity of lower trace 0.05V/cm.

In operation, the target surface is kept at a positive potential E with respect to the electrically grounded drift tube. A positive potential E' is also applied to the decelerating grid, while the front of the detector is at a negative potential E''.

Ions produced by irradiation of the target with the output of the laser are accelerated into the drift tube, where mass separation is achieved simply because ions of different masses have acquired different velocities under the action of the same accelerating potential difference. Upon leaving the drift tube, the ions are decelerated by the positive potential applied to the grid, and if they surmount the potential E', are finally accelerated into the detector. The multiplier current is measured across a 220 ohm resistor, giving a detector time constant of $\leq 10^{-7}$ seconds.

Experimental Details

A ruby laser with a cryptocyanine Q-switch was used in all the experiments. The output of the laser consists of a nearly triangular pulse with a full width of 30 nanoseconds at the base, and peak power of 6 Mw. The light flux at the target was 20-70 Mw/cm^2 depending on the lens used to focus the beam.

The experimental arrangement is shown in Figure 2. The laser is aimed at the surface through a sapphire window in the spectrometer envelope, at an angle of 53 degrees to the normal. The signal from the electron multiplier measuring the ion current in the time-of-flight spectrometer is fed to the two vertical inputs of a Tektronix 555 dual beam oscilloscope. Time base A of the scope is triggered by the signal from a Raytheon 917 phototube monitoring the laser pulse. Time base B is triggered internally by the electron multiplier signal after a variable delay time has elapsed, provided that B has been preconditioned by the triggering of time base A. The gate outputs of time bases A and B are fed into the start and stop inputs of a CMC-800A digital counter. Different mass pulses can be measured by simply varying the trigger delay on time base B. The output of the 917 photodiode is also used to trigger a Tektronix 585 oscilloscope that displays the output of a Philco 4501 diode monitoring the laser pulse.

Ion Energies

Figure 3 shows spectra obtained from a tungsten surface irradiated with a flux of 50 Mw/cm^2, and held at a positive potential $E = +1000V$. The upper trace shows the laser pulse; the lower trace is the multiplier signal. Time increases to the left.

Figure 3a was taken with $E' = E = +1000V$, i.e., no net decelerating potential. Under these conditions all ions emitted by the surface within the spectrometer aperture are collected. Figure 3b is taken under the same set of conditions

as 3a, except that the potential of the decelerating grid has been increased to $E' = +1180V$., while $E = +1000V$. If E' is further increased to +1200V, while holding E constant at +1000V, all peaks disappear. The presence of the two major peaks in Figure 3b, that have been identified as Na^+ and K^+, indicates that some of the ions have energies in excess of 180 eV. On the other hand, the ability to block the pulses from reaching the detector by increasing E' assures that they are charged particles.

There are two other factors that support the existence of high energy ions. First, the number of ions per peak in Figure 3b is only 1% of the corresponding number in 3a. Second, it can be seen that the narrowing of the peaks of Figure 3b has occurred by the elimination of the low energy tail in the peaks of 3a.

At this point it seems worthwhile to consider possible sources of spurious signals that might appear to be high energy ions in the spectrometer. One may rule out the possibility of electrons generated anywhere in the system arriving at the detector, since they would have to surmount a potential barrier of 3-5 kilovolts immediately in front of the multiplier. Two other possible sources of spurious signals are UV emitted by the heated target, and ions generated at places other than the target. The former, if present, would be easily identified by a zero time-of-flight and an undiminished signal when a strong magnet is placed near the target. Ions generated at any point between the target and decelerating grid will not have the full energy normally given to ions in the accelerating region. Hence, they will not be able to surmount the decelerating barrier, since $E' > E$. Ions formed past the decelerating electrode will be accelerated to the detector and recorded, but they cannot be stopped by the decelerating potential. The fact that we are able to cut-off all the peaks by increasing E' indicates that this is not taking place.

Ion Masses

The time-of-flight of a particle of mass number m, from target to detector, can be calculated using simple equations of motion. For the spectrometer dimensions[7], the time of flight for a singly ionized particle is given by

$$
(1) \quad t \, (\mu sec) = 1.44\sqrt{m} \left\{ -\frac{1.5\sqrt{E_0}}{E} + \left(\frac{1.5}{E} + \frac{50.0}{E_0 + E} + \frac{0.3}{E'} \right)\sqrt{E_0 + E} \right.
$$

$$
\left. \left(\frac{0.3}{E'} + \frac{0.6}{E''} \right)\sqrt{E_0 + E - E'} + \frac{0.6}{E''}\sqrt{E_0 + E - E' + E''} \right\}
$$

where E_o is the initial energy of the particles (in ev) and E, E', and E'' are the absolute values of the voltages (in volts) applied to the electrodes, as shown in Figure 2. Figure 4 shows the time of flight of particles of different charge to mass ratio as a function of initial energy E_o, for E' = E = 1000V and E'' = -3000V. It can be seen from the figure that the resolution of the instrument is large enough that, for the values of m/e shown, no serious overlap of peaks is expected for initial energies in excess of 100 eV. Hence, even in the absence of an energy analyzer, the peaks will be well enough resolved to make mass assignments possible. This fact is clearly demonstrated by the well resolved peaks shown in Figure 3.

Table I compares the measured and calculated times of flight for the masses found in the emission from the tungsten surface.

TABLE 1

ION MASSES FROM TIME OF FLIGHT

Mass	Ionic Species	Measured TOF (μs)	Calculated TOF (μs)
1	H^+	2.5	2.4
7	Li^+	6.4	6.4
12	C^+	8.3	8.3
18	H_2O^+	10.1	10.2
23	Na^+	11.9	11.6
28	CO^+	13.3	12.8
39	K^+	15.7	15.0
44	CO_2^+	16.7	16.0
184	W^+	33.0	32.7

The times of flight were calculated using (1) with E = +1000V, and assuming singly charged thermal ions. A correction for the fringing of the accelerating field is included[7].

There are several reasons for assuming that the ions observed are singly charged. First, the assumption leads one to mass assignments for the observed peaks that are in agreement with the results of electron and laser beam probing of polycrystalline tungsten surfaces in sector[8] and quadrupole[9] mass spectrometers respectively. Second, if the particles were doubly charged, one would expect to see a larger peak at the time corresponding to the arrival of singly charged ions of the same species. This is not found in any of our measurements.
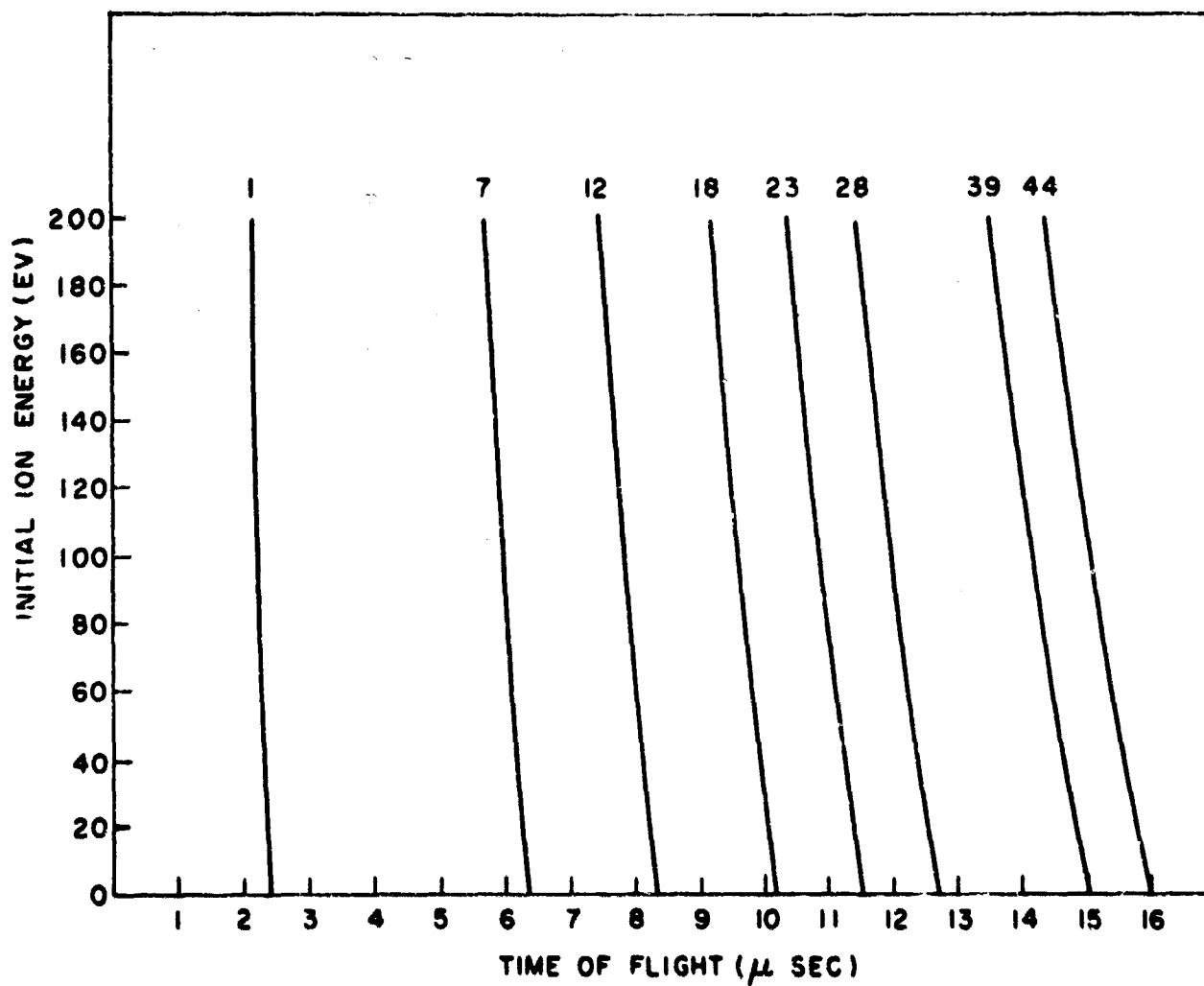
Figure 4 Appendix II - Time of Flight vs. Initial Ion Energy

While the presence of large quantities of alkali metals may seem surprising, they are a common contaminant in tungsten, for their compounds are used in the processing of tungsten ore and the rolling of the metal. The other ionic species found are known to adsorb readily or metal surfaces.

Number of Ions

The number of ions of different species that are emitted per laser pulse have been measured by integration over peaks such as those in Figure 3. The calibration procedure for the spectrometer has been given elsewhere [7]. Typical numbers for a light flux of 70 Mw/cm^2 are 9×10^8 K$^+$, 2×10^8 Na$^+$ and 2×10^8 W$^+$ ions respectively. These three ionic species make up most of the emission from the heated surface. The relative numbers of ions do not represent the relative abundance of different species in the emission, since the alkali metals will boil off the tungsten primarily as ions. In fact, measurements of the neutral particle emission made in a quadrupole spectrometer [9] for the same laser powers indicate that there are approximately 10^{13} particles emitted per pulse. This also means that we are dealing with a lightly ionized gas, which explains why the ions react readily to external electric fields.

The number of W$^+$ ions measured per pulse has been compared with the number predicted by the Saha equation [10] for a tungsten surface at the temperature of the target. The temperature of the surface, as well as the number of electrons emitted at that temperature, were calculated by methods previously described [1]. The number of tungsten ions was then calculated using known mass evaporation rates [11]. The number of ions predicted by the Saha equation using the values obtained from the above calculations is 10^5. Hence, we see that the numbers of ions is considerably higher than would be expected from a purely thermal process.

Inverse Bremsstrahlung Heating

The question of the origin of the high energy ions and their acceleration mechanism is of interest. We have considered a number of possible mechanisms. To date there is no satisfactory description of the processes in which these ions originate. The mechanism which produces high energy ions must operate quite generally, since they are produced under a wide variety of experimental conditions. The ion velocities obtained in the present experiment are in fact comparable to those observed when much higher laser power densities are employed. [3]

Many workers[12] have considered the importance of absorption by inverse Bremsstrahlung in heating a laser produced plasma. While this process is capable of producing considerable heating in a dense plasma, it does not appear to be operative in producing the ions observed here[13]. However, because of the great present interest in this process, both for producing hot dense plasmas and for contributing to the growth of laser produced gas breakdown, it is worthwhile to develop the reasoning leading to the present negative result.

The early portion of the laser pulse vaporizes material which is emitted as a plasma. Since the power density under our experimental regime is relatively low and since the surface is not extensively damaged, we assume the material is relatively cool, in equilibrium with the relatively slowly vaporizing surface, and is only slightly ionized. A fraction of the later part of the laser pulse is absorbed in the plasma by absorption of a photon by a free electron in the plasma in the inverse Bremsstrahlung process. The previous workers[12], considering a hot dense plasma as the starting point, have showed that this interaction can provide considerable heating, to the point where hundreds of electron volts per ion of thermal energy are produced.

However, these results are not necessarily applicable in our conditions. We can indeed envision a heating process of this type in our postulated plasma. The presence of a small amount of ionization leads to a small amount of heating which in turn leads to an increase in ion density through thermal ionization. This causes an increase in the absorption coefficient, and hence a higher rate of heating, so that the process leads to a rapid runaway heating. The process is opposed by expansion of the plasma, which lowers the particle densities, and by radiation of energy from the plasma, which lowers the temperature. The ion density must eventually be limited by the total number of heavy particles present.

The absorption coefficient k_ν for absorption of light of frequency ν by inverse Bremsstrahlung in a plasma of singly changed ions of density n_i and electrons of density n_e including cooperative effects in the plasma is given by[14]

$$k_\nu = \frac{8 \pi n_e n_i e^6 \ln \Lambda}{3 e \nu^2 (2 \pi m kT)^{3/2}}$$

where e and m are the electronic mass and charge, T the plasma temperature, and k is Boltzmann's constant. Here Λ is given by:

$$\Lambda = \frac{3 \pi n_e}{2 e^3} \left(\frac{kT}{\pi n_e} \right)^{3/2}$$

Over a broad range of temperatures and electron densities covering the range of interest, $\ln \Lambda$ is approximately equal to 10.

The expansion of the plasma is assumed to proceed as a complete rarefaction wave[15]. We assume initial conditions for the material with respect to particle densities and temperature. We assume the material is in equilibrium with the surface and that the ion density is given by the Saha equation[11], i.e., that collisional processes in the blowoff material occur sufficiently rapidly to keep the ion concentration in equilibrium with the temperature and the other particle densities. This assumption is open to serious question for our experimental situations however, if it does not accurately describe the situation, the actual temperature will be lower than what we calculate here and the conclusions of this analysis will be unchanged.

For a volume of blowoff material beginning to expand near the target, k_v can be calculated and thus the rate of heating due to the absorption of radiation can be determined from the initial particle densities. Then the changes in particle densities are calculated from the equations describing the rarefaction process and the Saha relation. The heating rate can then be redetermined from the revised value of k. Thus the ionization, expansion, and heating of a volume element of blowoff material can be followed as a function of time starting from its initial condition at the surface of the target. This computational routine has been carried out on a computer.

Results for two sets of initial conditions appear in Figure 5a and 5b. The initial electron density is an independent parameter. The initial neutral molecule density is different in the two parts of the figure.

We see that for considerable heating to occur, the electron density must be relatively high. At low electron densities there is practically no heating effect. As electron density is increased, we reach a point where a rapid nonlinear heating occurs. The increases in temperature and ion density interact on each other an increase in either quantity drives the other upwards even faster. There appears to be a critical electron density above which the process is possible and below which only slight heating occurs. In this particular case, an initial electron density of the order of 10^{19} cm^{-3} is necessary to result in this process occurring during a 30 nanosecond laser pulse. Changes in the other initial parameters, the temperature and the neutral particle density, have only a small effect on the behavior of the system, although they do determine the value of the critical electron density. Comparison of Figure 5a with Figure 5b shows that the critical electron density increases as initial particle density decreases although the variation is not extremely sensitive. The values of initial neutral density used in Figures 5a and 5b bracket a range in which the actual value may be expected to fall. We shall estimate an upper limit to this value next
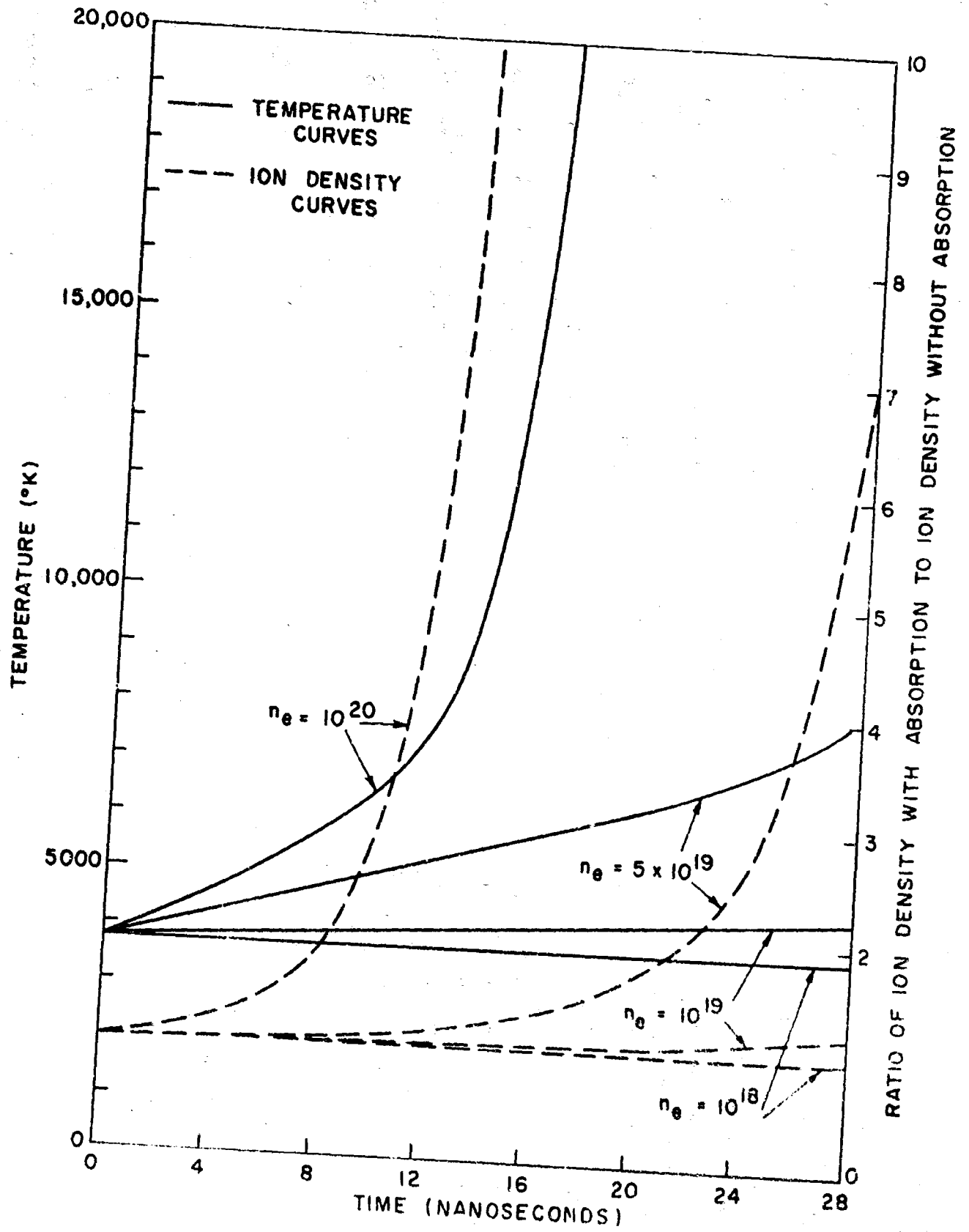
Figure 5a Appendix II — Initial Neutral Particle Density 10^{14} cm^{-3}
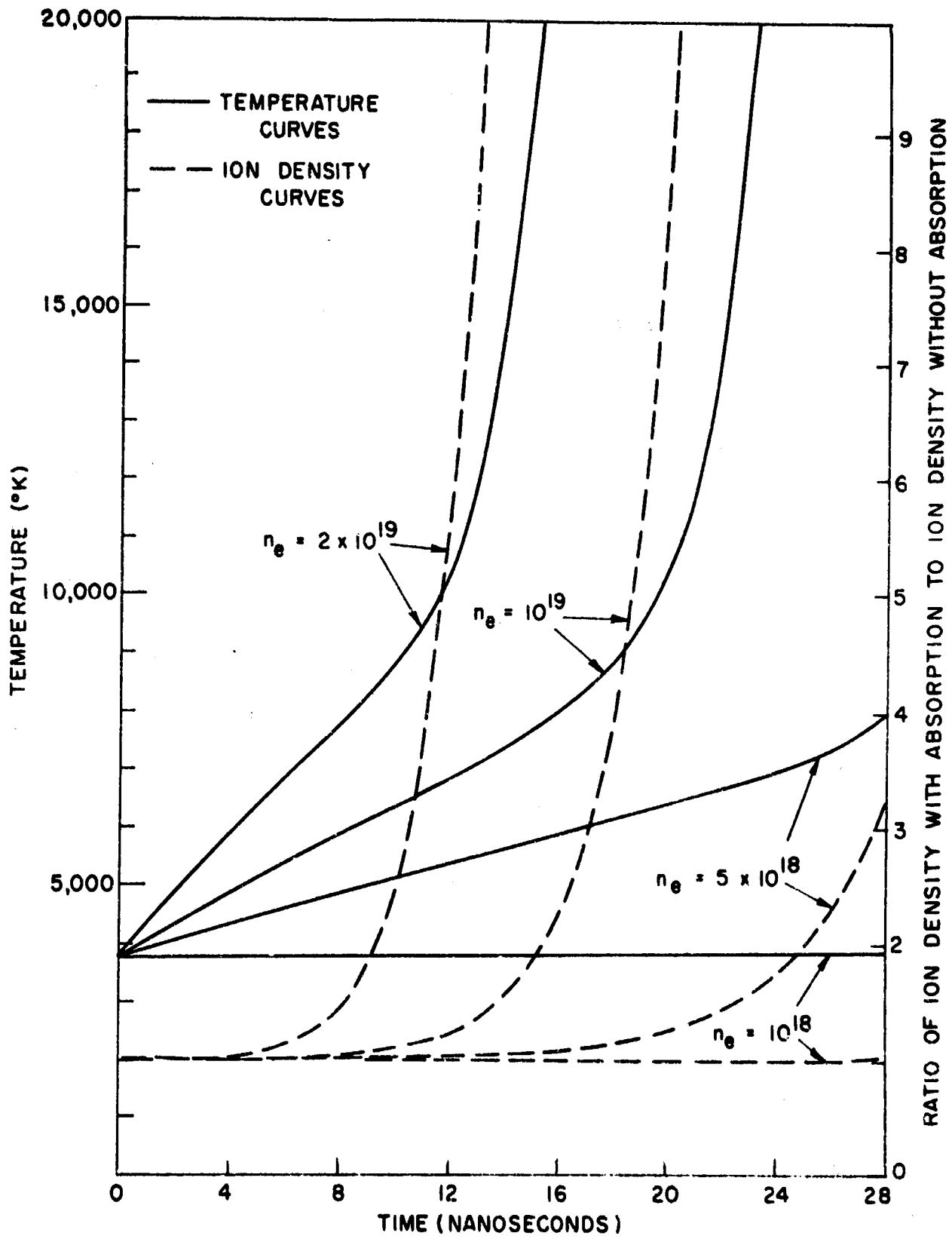
Figure 5b Appendix II - Initial Neutral Particle Density 10^{19} cm^{-3}

We may calculate an upper limit to the initial density of neutral particles[1] by calculating the amount of material vaporized by the laser theoretically[1]. Using techniques described in reference 1, we calculate a vaporized depth of 5×10^{-7} cm for our present experimental situation. At a thermal velocity of 10^5 cm/sec, this would lead to a neutral particle density of 4×10^{18} cm^{-3}. The depth of material removed per pulse can also be measured by striking the same spot with a number of identical laser pulses and then dividing the depth of the hole produced by the number of pulses. We carried out this measurement using a metallograph. Because of lack of sensitivity in measuring very small depths, we determined only an upper limit to the depth removed. For the present experiment, we determine that the depth removed per pulse must have been less than 10^{-6} cm, in reasonable agreement with the value calculated above. We note that the results in Figures 5a and b bracket a range of initial neutral particle density consistent with these results.

We have in this analysis shown that inverse Bremsstrahlung can lead to heating of the blowoff material under certain conditions, the most important of which is a high initial electron density. However, for our experimental conditions, the required electron density is too high to allow for this process to proceed. From measurements of the thermionic emission current produced by a Q switched laser[2] with thermal electron velocities in equilibrium with the surface, we estimate a realistic electron density in the range 10^{14} - 10^{15} cm^{-3} for our experimental conditions. The numbers of electrons emitted were obtained under conditions in which the accelerating voltage was large enough to overcome space charge effects.

The results quoted earlier in the section on numbers of ions establish that the gas is very lightly ionized. This result, taken in conjunction with the above upper limit for neutral particle emission, support the result that the initial electron density must be orders of magnitude lower than $10^{18}/\text{cm}^3$.

Thus the picture most consistent with experimental results for the range of laser power densities 20-70 megawatts/cm^2 is that of a slightly ionized gas. The ions and electrons are produced along with a larger number of neutral atoms and molecules. The initial electron densities are too low to lead to plasma heating by the processes described above. The calculated results do appear to be qualitatively similar to what is observed with higher laser powers, where the critical particle densities may be attained. Further investigations of the production mechanism in this range of laser powers should apparently consider means of producing high directed energies rather than high thermal energies for the ions.

Acknowledgements

REFERENCES FOR APPENDIX II

1) Ready, J. F., Effects Due to Absorption of Laser Radiation, J. Appl. Phys., Vol. 36, Feb. 1965, pp. 462-468.

2) Ready, J. F., Mechanism of Electron Emission Produced by a Giant Pulse Laser, Phys. Rev., Vol. 137, Jan. 1965, pp. A620-A623.

3) Linlor, W. I., Ion Energies Produced by Laser Giant Pulse, Appl. Phys. Letters, Vol. 3, Dec. 1963, pp. 210-211.

4) Linlor, W. I., Some Properties of Plasma Produced by Laser Giant Pulse, Phys. Rev. Letters, Vol. 12, April 1964, pp. 383-385.

5) Isenor, N. R., Metal Ion Emission Velocity Dependence on Laser Giant Pulse Height, Appl. Phys. Letters, Vol. 4, April 1964, pp. 152-153.

6) Opower, H., and E. Burlefinger, Temperature Determination of Plasmas Produced by Giant Laser Pulses, Phys. Letters, May 1965, pp. 37-38

7) Bernal G., E., L. P. Levine, and J. F. Ready, Time-of-Flight Spectrometer for Laser-Surface Interaction Studies, Rev. Sci. Inst., Vol. 37, July 1966.

8) Lichtman, D., private communication.

9) Levine, L. P., J. F. Ready, and E. Bernal G., unpublished results.

10) Landau, L. D., and E. M. Lifshitz, Statistical Physics, Addison-Wesley, Reading, Mass., 1958.

11) Jones, H. A., and I. Langmuir, The Characteristics of Tungsten Filaments as Functions of Temperature, G. E. Review, Vol. 30, 1927, pp. 2-22.

12) Dawson, J. M., On the Production of Plasma by Giant Pulse Lasers, Phys. Fluids, Vol. 7, July, 1964, pp. 981-987 Basov, N. G., and O. N. Krokhin, Conditions for Heating Up of a Plasma by the Radiation from an Optical Generator, J. Expt. Theoret. Phys (USSR) Vol. 46, January, 1964, pp. 171-175 [Translation in Soviet Phys - JETP, Vol 19, July, 1964, pp. 123-125]; Tozer, B A., P. R. Smy, and J. K. Wright, The Production of High Temperature Plasmas by Intense Laser Pulses, Proc. Phys. Soc., Vol. 86, July, 1965, pp. 45-51 Browne, P. F., Mechanism of Gas Breakdown by Lasers, Proc. Phys. Soc., Vol 86, Dec., 1965, pp 1323-1332

13) Ready, J. F., L. P. Levine, and E. Bernal G., Mechanisms of Particle Emission Produced by the Interaction of High Power Laser Radiation with Tungsten Surfaces, Paper presented at the Eighteenth Annual Gaseous Electronics Conference, October 20-22, 1965, Minneapolis, Minn.

14) Dawson, J. M., and C. R. Oberman, High Frequency Conductivity and the Emission and Absorption Coefficients of a Fully Ionized Plasma, Phys. Fluids, Vol. 5, May 1962, pp. 517-524.

15) Courant, R., and K. O. Friedrichs, Supersonic Flow and Shock Waves, Interscience, 1948, Ch. III.

ERRATA

FOR

FINAL REPORT CONTRACT NO. DA-11-022-AMC-1749(A) MOD NO. 2
MECHANISMS OF LASER SURFACE INTERACTIONS

Page 5: 10 microseconds/cm should read 8.5 microseconds/cm.

Page 10: Lines 10 through 20 should be replaced by:

$$R = 144 \left[\frac{ME}{B^2} \right]^{1/2}$$

where R is the radius of curvature of the trajectory in cm, E is the particle energy in ev, B is the field in gauss, and m is the mass in atomic mass units. For B = 500 gauss, E = 200 ev, and m = 50 amu, R is about 30 cm. Since this 500 gauss field could be applied over an area encompassing at least 5 cm of particle path length; it should be possible to deflect such ions approximately 0.5 centimeter. Since this distance is about equal to the separation between the quadrupole rods, it should be possible to deflect these particles out of the system. The conclusion is even stronger for particles of smaller mass. Thus it should be possible to stop even relatively fast ions with the magnetic field. In the experiments described below both methods (mass filter and magnetic field) were used.

Page 28: Equation II-11, w should read w'. Third line from bottom should read: where w' = initial ion velocity plus velocity imparted by field between target and grid.

Page 36: w should be replaced by w in both the ordinate and abscissa.

Page 37: w should be replaced by w in both the ordinate and abscissa.

Page 42: 40×10^6 in the abscissa should read 40×10^5.

DOCUMENT CONTROL DATA - R&D

(Security classification of title, body of abstract and indexing annotation must be entered when the overall report is classified)

1. ORIGINATING ACTIVITY (Corporate author)	2a. REPORT SECURITY CLASSIFICATION
Honeywell Inc. Corporate Research Center Hopkins, Minnesota	Unclassified
	2b. GROUP

3. REPORT TITLE

MECHANISMS OF LASER-SURFACE INTERACTIONS

4. DESCRIPTIVE NOTES (Type of report and inclusive dates)

Final Report

5. AUTHOR(S) (Last name, first name, initial)

Ready, J.F.; G., E. Bernal; and Levine, L.P.

6. REPORT DATE	7a. TOTAL NO. OF PAGES	7b. NO. OF REFS
May 1966	96	24

8a. CONTRACT OR GRANT NO.	9a. ORIGINATOR'S REPORT NUMBER(S)
DA-11-022-AMC-1749(A) Mod. No. 2	
b. PROJECT NO.	
c.	9b. OTHER REPORT NO(S) (Any other numbers that may be assigned this report)
d.	

10. AVAILABILITY/LIMITATION NOTICES

Distribution of this document is unlimited.

11. SUPPLEMENTARY NOTES	12. SPONSORING MILITARY ACTIVITY
	U.S. Army Ballistic Research Laboratories Aberdeen Proving Ground, Maryland

13. ABSTRACT

The work described in this report deals with the measurement of particle emission from metal surfaces irradiated with light flux densities of 50-70 Mw/cm^2, as well as calculations of the velocity distribution of the particles from the measured pulse shapes. Measurements in the quadrupole mass spectrometer have shown that, besides the thermal gas desorption, the neutral particle emission contains a photon pulse and several high velocity non-zero-mass pulses. Tentative assignments of masses and energies of the high speed neutral pulses are made.

99

DD FORM 1473
1 JAN 64

14. KEY WORDS	LINK A		LINK B		LINK C	
	ROLE	WT	ROLE	WT	ROLE	WT
Detector						
Control						
Effects						
Adsorption						
Surfaces						
Mass Spectroscopy						

INSTRUCTIONS

1. **ORIGINATING ACTIVITY:** Enter the name and address of the contractor, subcontractor, grantee, Department of Defense activity or other organization *(corporate author)* issuing the report.

2a. **REPORT SECURITY CLASSIFICATION:** Enter the overall security classification of the report. Indicate whether "Restricted Data" is included. Marking is to be in accordance with appropriate security regulations.

2b. **GROUP:** Automatic downgrading is specified in DoD Directive 5200.10 and Armed Forces Industrial Manual. Enter the group number. Also, when applicable, show that optional markings have been used for Group 3 and Group 4 as authorized.

3. **REPORT TITLE:** Enter the complete report title in all capital letters. Titles in all cases should be unclassified. If a meaningful title cannot be selected without classification, show title classification in all capitals in parenthesis immediately following the title.

4. **DESCRIPTIVE NOTES:** If appropriate, enter the type of report, e.g., interim, progress, summary, annual, or final. Give the inclusive dates when a specific reporting period is covered.

5. **AUTHOR(S):** Enter the name(s) of author(s) as shown on or in the report. Enter last name, first name, middle initial. If military, show rank and branch of service. The name of the principal author is an absolute minimum requirement.

6. **REPORT DATE:** Enter the date of the report as day, month, year; or month, year. If more than one date appears on the report, use date of publication.

7a. **TOTAL NUMBER OF PAGES:** The total page count should follow normal pagination procedures, i.e., enter the number of pages containing information.

7b. **NUMBER OF REFERENCES:** Enter the total number of references cited in the report.

8a. **CONTRACT OR GRANT NUMBER:** If appropriate, enter the applicable number of the contract or grant under which the report was written.

8b, &, & 8d. **PROJECT NUMBER:** Enter the appropriate military department identification, such as project number, subproject number, system numbers, task number, etc.

9a. **ORIGINATOR'S REPORT NUMBER(S):** Enter the official report number by which the document will be identified and controlled by the originating activity. This number must be unique to this report.

9b. **OTHER REPORT NUMBER(S):** If the report has been assigned any other report numbers *(either by the originator or by the sponsor)*, also enter this number(s).

10. **AVAILABILITY/LIMITATION NOTICES:** Enter any limitations on further dissemination of the report, other than those imposed by security classification, using standard statements such as:

(1) "Qualified requesters may obtain copies of this report from DDC."

(2) "Foreign announcement and dissemination of this report by DDC is not authorized."

(3) "U. S. Government agencies may obtain copies of this report directly from DDC. Other qualified DDC users shall request through

_____ ."

(4) "U. S. military agencies may obtain copies of this report directly from DDC. Other qualified users shall request through

_____ ."

(5) "All distribution of this report is controlled. Qualified DDC users shall request through

_____ ."

If the report has been furnished to the Office of Technical Services, Department of Commerce, for sale to the public, indicate this fact and enter the price, if known.

11. **SUPPLEMENTARY NOTES:** Use for additional explanatory notes.

12. **SPONSORING MILITARY ACTIVITY:** Enter the name of the departmental project office or laboratory sponsoring *(paying for)* the research and development. Include address.

13. **ABSTRACT:** Enter an abstract giving a brief and factual summary of the document indicative of the report, even though it may also appear elsewhere in the body of the technical report. If additional space is required, a continuation sheet shall be attached.

It is highly desirable that the abstract of classified reports be unclassified. Each paragraph of the abstract shall end with an indication of the military security classification of the information in the paragraph, represented as *(TS), (S), (C),* or *(U)*.

There is no limitation on the length of the abstract. However, the suggested length is from 150 to 225 words.

14. **KEY WORDS:** Key words are technically meaningful terms or short phrases that characterize a report and may be used as index entries for cataloging the report. Key words must be selected so that no security classification is required. Identifiers, such as equipment model designation, trade name, military project code name, geographic location, may be used as key words but will be followed by an indication of technical context. The assignment of links, rules, and weights is optional.